Accepted Manuscript

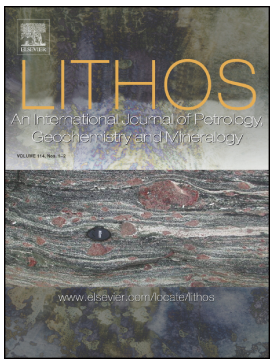

Constraints on lithosphere-asthenosphere melt mixing in basaltic intraplate volcanism from olivine melt inclusions from southern Payenia, Argentina

Nina Søager, Maxim Portnyagin, Kaj Hoernle, Paul Martin Holm, Dieter Garbe-Schönberg

PII: S0024-4937(18)30138-5
DOI: doi:10.1016/j.lithos.2018.04.011
Reference: LITHOS 4627

To appear in:

Received date: 6 November 2017
Accepted date: 13 April 2018

Please cite this article as: Nina Søager, Maxim Portnyagin, Kaj Hoernle, Paul Martin Holm, Dieter Garbe-Schönberg , Constraints on lithosphere-asthenosphere melt mixing in basaltic intraplate volcanism from olivine melt inclusions from southern Payenia, Argentina. The address for the corresponding author was captured as affiliation for all authors. Please check if appropriate. Lithos(2018), doi:10.1016/j.lithos.2018.04.011

This is a PDF file of an unedited manuscript that has been accepted for publication. As a service to our customers we are providing this early version of the manuscript. The manuscript will undergo copyediting, typesetting, and review of the resulting proof before it is published in its final form. Please note that during the production process errors may be discovered which could affect the content, and all legal disclaimers that apply to the journal pertain.

ACCEPTED MANUSCRIPT

Constraints on lithosphere-asthenosphere melt mixing in basaltic intraplate volcanism from olivine melt inclusions from southern Payenia, Argentina

Nina Søager[1,2]*, Maxim Portnyagin[1], Kaj Hoernle[1], Paul Martin Holm[2], Dieter Garbe-Schönberg[3]

[1]GEOMAR, Helmholtz Centre for Ocean Research, Wischhofsstraße 1-3, 24148 Kiel, Germany.

[2] University of Copenhagen, Department of Geosciences and Natural Resource Management, Øster Voldgade 10, Copenhagen DK-1350, Denmark.

[3]Kiel University, Christian-Albrechts-Platz 4, 24118 Kiel, Germany

*corresponding author. Tel.: +45 35332975, e-mail: ns@ign.ku.dk

ACCEPTED MANUSCRIPT

Abstract[1]

We present major and trace element compositions of melt inclusions from three alkali basalts from the Río Colorado volcanic field in the Payenia backarc province, Argentina. Modeling of diffusion profiles around the inclusions showed that most inclusions equilibrated less than 14 days after formation, indicating a short crustal residence time for the magmas and nearly direct ascent through the crust. Despite overlapping host rock isotopic compositions, the inclusions show a large variation in their degree of enrichment, and display trends that we interpret as mixing between asthenospheric OIB-type low K_2O-high Nb/U melts and enriched high K_2O-low Nb/U lithospheric mantle melts similar in composition to alkaline lamprophyres. The low Nb/U magmas are excessively enriched in the elements Cs, Rb, Ba, Th, U, K, Pb and Cl relative to Nb, Ta and REEs. The enriched

[1] Abbreviations: wr –whole rock, SVZ –Southern Volcanic Zone of the Andes, UCC –upper continental crust average

ACCEPTED MANUSCRIPT

low Nb/U components are interpreted to have formed by percolative fractional crystallization of asthenospheric high Nb/U melts in the lithospheric mantle involving crystallization of clinopyroxene, apatite and rutile. The residual fluid-rich melts either mixed directly with new batches of high Nb/U melts or metasomatized and veined the lithospheric mantle which later re-melted during continued volcanism. The major element compositions of the high K_2O-low Nb/U components are distinct for the whole rocks and melt inclusions, and most enriched inclusions have lower SiO_2 and higher TiO_2 contents indicating derivation by melting of amphibole-bearing veins. In contrast, most wr low Nb/U basalts have higher SiO_2 and lower TiO_2 and were most likely formed by melting of pyroxenitic veins or peridotitic metasomatized lithospheric mantle.

Keywords: Intraplate basalts, melt inclusions, olivine, lithospheric mantle, alkaline lamprophyres

Introduction

It has long been recognized that asthenospheric mantle melts may interact with the lithospheric mantle to various extents during transit through oceanic or continental lithosphere and that the interaction changes the composition of the melts and metasomatizes the lithospheric mantle (e.g. Bedini et al., 1997; Foley et al., 1992b; Harte et al., 1993; McKenzie, 1989; Pilet et al., 2005, 2008; Wass and Rogers, 1980). It is, however, a continuous challenge to distinguish asthenospheric from lithospheric mantle melts and their relative contributions to intraplate magmas, in particular in the cases where there is little or no isotopic contrasts (e.g. Class and Goldstein, 1997; Le Roex and Lanyon, 1998; Simonetti et al., 1998; Pilet et al., 2005, 2008). The modeling by Bedini et al. (1997) and Pilet et al. (2011) showed that the process termed 'percolative fractional crystallization' (Harte et al., 1993) can produce changes in melt and mantle source trace element ratios such as

ACCEPTED MANUSCRIPT

Nb/U, Nb/La and Ce/Pb, otherwise assumed to be unaffected by melting and crystallization, due to crystallization of minor phases such as rutile and apatite which fractionate the trace element ratios. This process could therefore account for differences in trace element patterns between magmas with similar isotopic compositions.

One type of intraplate rocks generally regarded as of lithospheric mantle origin are the alkaline lamprophyres (as defined by Le Maître, 2002) such as camptonites and monchiquites. Alkaline lamprophyres are spatially and genetically associated with alkali basaltic volcanism and are typically found in continental rift valleys and intraplate settings (e.g. Batki et al., 2014; Bédard, 1994; Mitchell, 1994; Rock, 1991). They are believed to be products of prolonged crystallization of volatile-rich magmas where the volatiles were retained in the magmas, whereas alkali olivine basalts were formed from less volatile-rich or degassed magmas (Bédard, 1994; Mitchell, 1994). Many authors favor a lithospheric mantle origin but often invoke ocean island basalt (OIB)-type asthenospheric melts as metasomatizing agents (e.g. Aghazadeh et al., 2015; Foley, 1992a,b; Le Roex and Lanyon, 1998; Simonetti et al., 1998; Tappe et al., 2006), and in several cases the metasomatic agents have been proposed to be plume melts and fluids from an earlier phase of plume magmatism (Caroff et al., 1997; Lundstrom et al., 2003; Le Roex and Lanyon, 1998; Simonetti et al., 1998). Here we use melt inclusions from the southern Payenia province (Argentina) to investigate the role of asthenosphere melt-lithospheric mantle interaction and to constrain the composition of the possible lithospheric mantle melt mixing end-members. We show that the full melt compositional variability observed from low K_2O-high Nb/U basalts to higher K_2O-low Nb/U basalts can be found within single samples, suggesting late-stage mixing of asthenospheric melts with alkaline lamprophyre-like lithospheric mantle melts at shallow levels.

Melt inclusions in olivine can trap melts at an early stage of magmatic fractionation and in some cases trap highly chemically heterogeneous compositions within a single sample (e.g. Gurenko and Chaussidona,

ACCEPTED MANUSCRIPT

1995; Ren et al., 2005; Qian et al., 2015). In contrast to whole rock analyses, which represent possible aggregated melts and their phenocrysts, melt inclusions can preserve more chemically extreme compositions of the pre-aggregated melts which more closely reflect the primary melts (Danyushevsky et al., 2000; Ren et al., 2005; Sobolev et al., 2000). They are therefore a valuable tool to investigate magma mixing processes and to trace mantle source variations at a smaller scale.

In order to examine the genetic relationship and trace the mantle sources of high and low Nb/U intraplate magmas from the Río Colorado volcanic field, which form part of the Quaternary Payenia volcanic province (34-38°S) in Argentina, we present major and trace element data on melt inclusions in olivine from three samples otherwise previously analyzed by Søager et al. (2015b). We argue that the varying trace element enrichment observed in the melt inclusions reflect mixing between EM1-type asthenospheric melts and enriched alkaline lamprophyric-type melts from metasomatized lithospheric mantle formed during the early stages of volcanism.

Geological setting

The Payenia volcanic province is situated in the backarc of the Andean Southern Volcanic Zone (SVZ) and covers more than 40,000 km^2 and includes more than 800 eruptive centres (Fig. 1). Together with the Auca Mahuida volcanic field, the Río Colorado volcanic field forms the southeasternmost part of the volcanic province furthest away from the SVZ volcanic front. The Nazca plate subducts at an angle of ~30° (Kendrick et al., 2003) and reaches a depth of ~300 km beneath the Río Colorado volcanic field. The Río Colorado volcanic field was active between 1.5 and 0.3 Ma and mainly consists of scattered basaltic monogenetic cones and small lava flows (Bertotto et al., 2006; Gudnason et al., 2012; Kay et al., 2006b), while the much more voluminous Auca

ACCEPTED MANUSCRIPT

Mahuida shield volcano was active between 1.8 and 0.9 Ma (Kay et al., 2006a; Rosello et al., 2002). The sampled cones are positioned along the Colorado river around 37.3°S and 69.0°W just north of the town Ríncon de los Sauces about 500 km behind the Chile trench. The cones overlie the Mesozoic to Paleogene sediments of the Neuquén basin (e.g. Vergani *et al*., 1995). The crust in the area has a thickness of ~40 km and the total lithospheric thickness is ~80 km (Gilbert *et al*., 2006; Tassara *et al*., 2006). Two samples (124570 and 124567) come from a polygenetic cone complex on the north side of the river with numerous generations of smaller lava flows which were mainly formed between 1 and 0.3 Ma (Gudnason et al., 2012). The last sample (CL467) was taken south of the Pata Mora bridge in a monogenetic cone probably of similar age as the youngest parts of the aforementioned cone complex.

The volcanism in Payenia started in the earliest Miocene where large amounts of OIB-like intraplate basalts were erupted in the southern part (Dyhr et al., 2013a, 2013b; Kay and Copeland, 2006). Due to a slab-shallowing during the middle Miocene to late Pliocene, the arc was shifted eastwards and arc and backarc volcanism occurred in large parts of the Payenia province (e.g. Bermudez et al., 1993; Dyhr et al., 2013b; Kay et al., 2004, 2006a, 2006b; Søager et al., 2013). During the Pliocene, the Nazca slab south of Payenia detached close to the trench and sank (Pesicek et al., 2012). Around the same time, the shallow slab beneath Payenia began to steepen. The steepening presumably started in the south and gradually progressed northwards (Gudnason et al., 2012; Kay et al., 2006a) and was accompanied by extensional tectonics (Folguera et al., 2008; 2009; Ramos and Folguera, 2011). As a result, strong upwelling of deep mantle over the southeastern edge of the slab beneath Payenia can explain the resumption of OIB-like intraplate magmatism in the southern part of the province, whereas slab-fluid enriched alkaline backarc volcanism dominated in northern Payenia (Dyhr et al., 2013a; Espanon et al., 2014; Folguera et al., 2009; Germa et al., 2010; Gudnason et al., 2012; Jacques et al., 2013; Kay et al., 2013; Søager et al., 2013, 2015b; Kay et al., 2006a).

ACCEPTED MANUSCRIPT

Previous work

The eruptive products found in the Río Colorado region are mainly trachybasalts and alkali basalts, but basanites also occur. Some of the Río Colorado basalts have the most OIB-like trace element patterns on incompatible element diagrams of all Quaternary basalts in Payenia (e.g. negative Pb and minor to no negative Nb and Ta spikes) and contain little or no input from the subducting slab (Jacques et al., 2013; Kay et al., 2013; Søager et al., 2013; Søager and Holm, 2013). The trace element and isotopic compositions of both the early Miocene and Pleistocene basalts are of EM1-type and show a large similarity in both major and trace element compositions to particularly the Gough Island basalts and South Atlantic E-MORB types such as Discovery and LOMU (Kay et al., 2013; Søager et al., 2013; Søager and Holm, 2013). Based on whole rock major element compositions and analyses of olivine compositions, the samples with the highest Nb/U (>~45) were suggested to be pure pyroxenite melts of an asthenospheric EM1-type source (Søager and Holm, 2013; Søager et al., 2015b). An electrical resistivity model has shown a deep mantle anomaly associated with the presence of melts and/or fluids extending from at least 400 km depth to the lithosphere beneath the Río Colorado volcanic field in southernmost Payenia (Burd et al., 2014). Søager et al., (2015b) suggested that the anomaly was created by upwelling and melting of pyroxenitic material from the mantle transition zone caused by the roll-back of the subducting oceanic plate.

The Río Colorado basalts fall in two compositional groups: a high Nb/U (41-60) and a low Nb/U (22-37) group, which have distinct major and trace element compositions but similar ranges of isotopic compositions (high Nb/U: $^{206}Pb/^{204}Pb$ 18.25-18.43, $^{87}Sr/^{86}Sr$ 0.70354-0.70378, $^{143}Nd/^{144}Nd$ 0.51279-0.51287; low Nb/U: $^{206}Pb/^{204}Pb$ 18.32-18.42, $^{87}Sr/^{86}Sr$ 0.70353-0.70391, $^{143}Nd/^{144}Nd$ 0.51279-0.51286) (Fig. 2) (Søager and Holm, 2013, 2015b). The low Nb/U basalts have higher contents of the most incompatible elements, higher K/La,

ACCEPTED MANUSCRIPT

Rb/Nb, Th/La, Zr/Sm and La/Sm than the high Nb/U basalts and lower Ce/Pb, and Ba/Th reflecting a larger enrichment in mainly K, Rb, Th and U relative to Ba, Nb, La and Ce (Fig. 2 and 3). The similar isotopic compositions, high U/Pb and low La/Nb of the two groups led to the conclusion that the trace element characteristics of the low Nb/U group was not caused by an input from the subducting slab because the slab influenced rocks from the arc and backarc of the Payenia region have more radiogenic Pb (>18.5), low U/Pb and high La/Nb (Søager and Holm, 2013). This was supported by the similarly low estimated oxygen fugacities for samples from the two groups (ΔQFM ~ 0), which were in contrast to the higher fugacities indicated for the slab-modified samples from other parts of Payenia (Søager et al., 2015b). Moreover, the slab fluid affected northern Payenia basalts were found to be peridotite melts with higher CaO than the pyroxenite-derived southern Payenia basalts, whereas the low Nb/U rocks have even lower CaO than the high Nb/U southern Payenia basalts suggesting a different origin than for the northern Payenia basalts (Fig. 3c). Søager et al. (2015b) calculated Al-in-olivine crystallization temperatures (Wan et al., 2008) for olivine-spinel pairs in the most extreme low Nb/U lava sample 126230. The temperatures exhibited a variation from temperatures similar to the other analyzed Río Colorado basalts (mainly above 1200°C) down to lower temperatures (down to 1126 °C) at similar or higher olivine forsterite contents. This was suggested to reflect mixing of hot asthenospheric melt with a lower temperature lithospheric mantle melt during crystallization of the olivines.

Of the samples analyzed in this study, one is of low Nb/U-type (124567) and two are of high Nb/U-type (124570 and CL4679). Whole rock major and trace elements and isotopes as well as most olivine compositions were published in Søager et al. (2015b).

ACCEPTED MANUSCRIPT

Description of melt inclusions

The measured inclusions range in size between 30 and 225 µm with most in the range 40-150 µm (Supplementary table A). They commonly have one or two vapor bubbles and small spinel crystals (Fig. 4). The glass is fresh and light to dark brown in color. Inclusions containing clinopyroxene crystals have been discarded. Sulfide globules are common in sample 124570 but only occur in a few inclusions in the other analyzed samples. Sulfide globules form due to a decreased S solubility in the melt as Fe re-equilibrates with the olivine walls (Danyushevsky et al., 2002). Therefore the measured S-contents should be considered to represent minimal initial values.

Analytical methods

Major element compositions of melt inclusions and matrices were analyzed using a JEOL JXA 8200 electron microprobe (EMP) at GEOMAR, Kiel, Germany. Analyses were run with an accelerating voltage of 15 kV, a current of 6 nA and 5 µm electron beam size. Counting time was 5/10 s (peak/background) for Na, 20/10s for Si, Al, Fe, Mg and Ca, 30/15 s for K, Ti, Cl and S and 40/20 s for Mn and F. For calibration and monitoring of data quality, natural and synthetic reference samples from the Smithsonian Institute (Jarosewich *et al.*, 1980) were run 2-3 times each for every 50-60 sample measurements and at the beginning and end of each analytical session. Results were normalized to these runs of basaltic glass (USNM 113498/1, VGA99) for Si, Al, Na, Mn, Ti, Fe, Mg, Ca and P, rhyolitic glass (USNM 72854, VG568) for K, and scapolite (USNM R6600-1) for S and Cl. The reproducibility of the standards is 1-7 % (2σ rel. %) for most elements except P_2O_5 (14.5 %) and MnO (46.7 %). In most cases, melt inclusions were measured twice and the reported compositions are averages of these. See results for samples in Supplementary table A and for standards in Supplementary table B.

ACCEPTED MANUSCRIPT

Olivine compositions were also measured at the EMP at Geomar, Germany, with an accelerating voltage of 15 kV, current of 100 nA and 1 µm electron beam size. Counting time was 60/30 s (peak/background) for Ca, 20/10s for Si, Fe and Mg, 30/15 s for Mn and Cr and 40/20 s for Al and Ni. For calibration and monitoring of data quality, the San Carlos olivine (USNM 11312/444; Jarosewich *et al*., 1980) was run 3 times for every 50-60 sample measurements and at the beginning and end of each analytical session. Results were normalized to the reference values for San Carlos olivine from Sobolev et al. (2007) and are listed in Supplementary table A and B. The reproducibility of the San Carlos Fo-numbers is 0.2 % (2σ rel. %).

Trace elements were determined by laser ablation – inductively coupled plasma – mass spectrometry (LA-ICP-MS) using a 193nm Excimer laser with a large volume ablation cell (ETH Zürich, Switzerland) coupled with an Agilent 7500s ICP-MS at the University of Kiel (CAU), Germany. Analyses were run with 44 µm pit size, 5 Hz pulse frequency and 10 J cm^{-2} fluence. The aerosol was transported with 1.3 L min^{-1} He and mixed with 1 l min^{-1} Ar prior to introduction into the ICP. The ICP-MS was operated under standard conditions at 1500W and optimized for low oxide formation (typically ThO/Th ≤ 0.4%). The GLITTER software package (Access Macquarie Ltd.) was used for data reduction of the time-resolved measurements which was done individually for each analysis. The blank signal was measured 20 s prior to each ablation and used for calculation of the actual detection limits. The analyzed isotopes are listed in Supplementary table C. ^{43}Ca was used for internal standardization utilizing data from EMP analyses. The NIST 612 glass (Jochum *et al*., 2011) and the MPI-DING standards KL2, BM90 and GOR128 (Jochum *et al*., 2006) were re-analysed in triplicate and duplicate, respectively, for every 30 sample acquisitions and in the beginning and end of each session. The inclusions were analysed in two sessions. The integrated raw data from the first session were calibrated using the BM90 and GOR128 standards and the second using KL2 and GOR128. The 2σ relative % deviations for 4 runs of the KL2 standard during the three sessions were below 13 % for most elements. Laser ablation data including standard measurements are given in Supplementary table C.

ACCEPTED MANUSCRIPT

Correction of melt inclusion major element compositions

The melt inclusion compositions have been corrected for post entrapment crystallization and Fe-loss by diffusion using PETROLOG3 (Danyushevsky and Plechov, 2011). The olivine-melt model used was from Danyushevsky (2001). fO_2 was set to ΔQFM = 0 at 1 atm pressure with Fe-oxidation model from Borisov and Shapkin (1990). The compatibility of Ca and Mn was set to zero.

Profiles of olivine compositions adjacent to the melt inclusions were measured for 16 inclusions from samples 124570, 124567 and CL467. The initial FeO^T-contents of the inclusions (FeOi) were modeled assuming instant cooling according to the method of Danyushevsky et al. (2000, 2002). The method is based on modelling the diffusive exchange of Fe and Mg between olivine and melt inclusion during pre-eruptive cooling and fitting the models to the measured olivine Mg#-profiles. The results provide estimates of FeOi in the melt inclusions and the degrees and duration times of the re-equilibration. The modelling was done to assess the extent of Fe-loss during post entrapment re-equilibration and the spread in FeOi values of the inclusions. If the inclusions have suffered severe Fe-loss or have a large spread in FeOi, the melt compositions may become either over or under-corrected by the post entrapment crystallization correction using whole rock (wr) FeO^T as FeOi of the inclusions and this will lead to erroneous results. The calculated models were initially fitted to the measured profiles by using the inclusion radius and wr FeO^T-contents and adjusting the cooling interval and % re-equilibration (see example in Fig. 5d). Subsequently, FeOi was found by varying the input FeO^T-content until the modeled FeO after diffusion equaled the measured FeO of the inclusions. Lastly, the cooling interval and % re-equilibration were re-fitted to match the estimated FeOi.

ACCEPTED MANUSCRIPT

The modeled FeOi values (Fig. 5a) were used to reconstruct the melt inclusion compositions at the time of trapping. For the inclusions where FeOi was not modeled, an average sample FeOi-content was calculated from the modeled values. For sample 124570, inclusion 2-58 was excluded from the average. The corrected compositions and model results are given in Supplementary table A.

The average modeled FeOi for samples 124567 and 124570 are very close to the wr FeO^T (Fig. 5a) indicating that the modeling is robust, but in particular in sample 124567 there is a considerable variation in the modelled FeOi between the inclusions. This variation reflects the overall much larger variability in the inclusion compositions of this low Nb/U-type sample relative to the inclusions of the high Nb/U-type samples 124570 and CL467 (Fig. 5c) which is interpreted as a result of incomplete mixing of mantle melts. For sample CL467, the average modeled FeOi is ~0.8 wt.% lower than the wr FeO^T. Since only three profiles have been modeled for this sample, this may be an artefact. However, this sample has accumulated significant amounts of olivine, as seen by the higher calculated equilibrium olivine forsterite content based on the wr composition (Fo_{87}) than the actual measured olivine compositions (Fo_{82-83}), and this would have increased the wr FeO^T due to the relatively low forsterite contents of the accumulated olivines. The difference in the corrected melt inclusion compositions using wr FeO and the modeled FeOi for the correction amounts to up to 1.2 wt.% MgO (Fig. 5c) with a difference between wr FeO^T and modeled FeOi of up to 1.5 wt.% (excepting inclusion 2-58). The results show that wr FeO^T is a good approximation to the FeOi for samples with homogenous melt inclusion compositions and with low amounts of accumulated crystals. However, in highly heterogeneous samples like 124567 or in samples with large amounts of accumulated crystals, using wr FeO^T as FeOi may lead to significant errors in the corrected melt inclusion compositions.

The modeled re-equilibration times range between 2 to 13 days for all but three inclusions (Fig. 5b), indicating short crustal residence times for the magmas and fast magma ascent rates. However, the

ACCEPTED MANUSCRIPT

equilibration profiles only record the time since the cooling event and therefore do not provide information about any possible crustal residence at constant temperature of entrapment. The only exception is inclusion 2-58 from sample 124570, which yields a residence time of 87 days. The host olivine has lower olivine forsterite contents than the other grains from this sample and the inclusion has a diverging trace element pattern relative to the other inclusions from this sample suggesting that this olivine is an antecryst. The Fe-Mg diffusion model does not account for the effect of H_2O which accelerates the diffusion rates of Fe and Mg in olivine (Hier-Majumder et al., 2005) and therefore the estimated re-equilibration times are maximum values. The short re-equilibration times are consistent with the primitive nature of the magmas and the mode of eruption in monogenetic cones. It is in good agreement with estimates of ascent times for Hawaiian basalts passing through a 100 km thick lithosphere by Maaløe (2011) who calculated ascent times of maximum 13-14 days for mantle nodule-bearing nephelinites and maximum 23 days for the tholeiitic basalts with olivine crystals up to 1 cm in diameter. The short equilibration times estimated for the Río Colorado samples similarly indicate close to direct ascent of the magmas through the lithosphere since entrapment of the melt inclusions.

Results

The melt inclusions have MgO-contents in the range 5.3-9.5 wt.% with inclusions from samples 124570 and CL467 having lower MgO than from sample 124567 (Fig. 6). Most inclusions were trapped in olivine of Fo_{79-87}. The fractionation paths shown with black lines show 8 % olivine fractionation to 6.5 wt.% MgO followed by 12.5 % fractionation of 80 % clinopyroxene + 20 % olivine to 5 % MgO. Wr high Nb/U sample 123972 (Søager et al., 2013) was used as starting composition and equilibrium olivine (assuming olivine $K_D^{(Fe/Mg)} = 0.30$ and $Fe^{2+}/FeO^T = 0.9$) and clinopyroxene were subtracted in steps of 0.5 %. The inclusions from each sample outline trends of increasing Al_2O_3 at decreasing MgO, indicating that plagioclase was not an important fractionating

ACCEPTED MANUSCRIPT

phase at the time of entrapment (Fig. 6a). The inclusions from sample 124570, which are the most evolved, do not show signs of decreasing CaO and CaO/Al_2O_3 with decreasing MgO indicating that they only experienced very limited amounts of clinopyroxene fractionation. Therefore, the melts of all inclusions are presumed to have evolved dominantly by olivine fractionation.

The trace element patterns of the inclusions from the high and low Nb/U samples (Fig. 7) are in most cases very similar to the wr patterns and typical for each group, but the inclusions from the low Nb/U sample (124567) have more variable patterns than the inclusions of the high Nb/U samples. There are a few exceptions though: Inclusion 5-33 from sample CL467 has a more enriched pattern and higher Ti and P than the other inclusions from this sample and the pattern is similar to the low Nb/U-type patterns of sample 124567 (Fig. 7b). The LA-ICP-MS analysis of this inclusion has 3290 ppm Cr, elevated contents of Zn, Co and Ni relative to the other inclusions from this sample and lower SiO_2 than the EMP analysis, suggesting entrapment of minor amounts of Cr-spinel during ablation. Due to the very low contents in Cr-spinels of the incompatible elements used in the trace element diagram (Fig. 7), the entrapment should not have affected the ratios between the incompatible elements. The Ti concentrations used in the plots are all from the EMP analyses. Inclusion 2-58 from sample 124570 (Fig. 7c) has a slightly different pattern than the other inclusions from this sample and the host olivine has lower Fo than most other olivines. This olivine is most likely an antecryst.

Both wr compositions with Mg# > 55 and all inclusions were fractionation corrected for equilibrium olivine fractionation/accumulation to MgO = 10 wt.% in steps of 0.1% (assuming olivine $K_D^{(Fe/Mg)} = 0.30$ and $Fe^{2+}/FeO^T = 0.9$) and were plotted in Fig. 8. The maximum difference between corrected and uncorrected concentrations amounts to 0.14 wt.% for K_2O and 0.3 wt.% for TiO_2 and the correction is therefore insignificant relative to the observed variation. The inclusions exhibit increasing K_2O correlated with decreasing SiO_2 and increasing Cl, S and P_2O_5 and in some cases TiO_2 (Fig. 8). The most extreme inclusion with highest K_2O and

ACCEPTED MANUSCRIPT

lowest SiO_2 from this trend is 5-33 from the high Nb/U sample CL467 (Fig. 8b), but otherwise the inclusions from the low Nb/U sample have the highest K_2O. However, at least two inclusions from sample 124567 diverge from this trend and have higher SiO_2 and lower TiO_2, CaO and CaO/Al_2O_3 at a given K_2O than the other inclusions from this sample, approaching a composition similar to the wr low Nb/U samples. The wr low Nb/U samples tend to have lower Dy/Yb ratios than the high Nb/U samples while the inclusions do not show a systematic variation (Fig. 8f). In Fig. 9 it can be seen that most of the low Nb/U inclusions have higher La/Sm and Rb/Sr and lower Ce/Pb, Ti/Eu and Ba/Th than the high Nb/U inclusions, while Th/U and U/Pb (not shown) fall within the same range.

Discussion

The overlapping isotopic compositions of the high and low Nb/U basalts (Fig. 2 and Søager and Holm, 2013) indicate that both groups were initially derived from the same source and that the enrichment processes happened relatively recently, because the low Nb/U basalts have higher Rb/Sr and lower Sm/Nd which would evolve to distinct Sr-Nd isotopic compositions with time. The isotopic compositions of the high and low Nb/U samples are distinct from those of the adjacent arc rocks (Fig. 2a) and from the subducting Pacific oceanic plate (Jacques et al., 2013; Søager and Holm, 2013). Furthermore, there is a distinct difference in major and trace element compositions between the slab flux metasomatized peridotite-derived melts (low FeO/MnO) from the northern Payenia (see also Søager et al., 2015b) and the Río Colorado low Nb/U component outlined by the trends of the wr low Nb/U samples towards higher Zr/Sm and K/La, constant La/Nb and lower CaO (Fig. 3). So despite the enrichment in fluid-mobile elements of the low Nb/U relative to the high Nb/U magmas, there are several lines of evidence (including those mentioned in the section *Previous work*) suggesting that the enriching component was not derived from the subducting slab.

ACCEPTED MANUSCRIPT

In terms of trace elements, the low Nb/U component is shifted towards the composition of evolved upper continental crustal rocks in several trace element ratios (shown in Fig. 9 as the global upper continental crustal average, UCC, from Rudnick and Gao, 2003), but assimilation of even small amounts of old upper crustal material would change the isotopic ratios of the Rio Colorado magmas, and therefore this explanation is at odds with the overlapping isotopic compositions in the two groups. Likewise, the higher Rb/Sr and lower Sm/Nd of the low Nb/U basalts means that their source would have developed distinct isotopic signatures if the high and low Nb/U sources were differentiated in an ancient event (>100 Ma), be it in the lithosphere or asthenosphere. Instead the enriched component most likely originated in the upwelling asthenospheric mantle generating the high Nb/U volcanism not long before eruption of the low Nb/U magmas.

There are a number of possibilities for a recent formation of the low Nb/U magmas/source. The low Nb/U melts could have formed from the asthenospheric high Nb/U mantle by processes such as lower degrees of melting, more extensive crystal fractionation, or melt-peridotite interaction involving phases such as amphibole, rutile or phlogopite which could potentially fractionate the trace element ratios in the observed way. Alternatively, the low Nb/U component could have been generated during the early Miocene Matancilla-Fortunoso volcanism or the Plio-Pleistocene Río Colorado volcanism in southern Payenia through metasomatism and veining of the lithospheric mantle by the asthenospheric melts. The much more heterogeneous trapped melt inclusion compositions of low Nb/U sample 124567 (Fig. 5-8) than in the other analyzed samples suggest that this was a poorly mixed magma that contained both high and low Nb/U melt-type components. Similarly, the temperatures recorded by the olivine-spinel pairs in the low Nb/U sample 126230 displayed a large range (~110 °C) from temperatures similar to the high Nb/U basalts to lower temperatures at roughly constant forsterite and Ni-contents of the olivines (Søager et al., 2015b). Both evidences indicate that the low Nb/U basalts are mixtures of mantle melts, of which one is probably a low temperature melt, mixing at a late stage during passage through the lithosphere. Whatever the case may be,

ACCEPTED MANUSCRIPT

any possible model should account for the differences in major element contents, degree of enrichment in incompatible elements and the different trace element patterns of the low and high Nb/U basalts.

Fractional crystallization of olivine, clinopyroxene and plagioclase in the crust cannot have generated the observed differences in the trace element patterns (Fig. 7), because the wr high and low Nb/U basalts have overlapping ranges of MgO suggesting largely equal degrees of fractionation and the mentioned minerals do not fractionate the highly incompatible elements in the observed way (Figs. 6 and 9). Furthermore, the melt inclusions from low Nb/U sample 124567 are both the most enriched in incompatible elements and the most primitive with highest MgO indicating that this is a feature of the primary melts. Lower degrees of mantle melting would generate melts with higher La/Sm, K_2O, TiO_2, P_2O_5 and Cl, and lower SiO_2 than higher degree melts and this could potentially explain the observed trends in Fig. 8. However, the two groups exhibit the same range in Zr/Nb and TiO_2-contents, suggesting similar degrees of melting because lower degrees of mantle melting would produce melts with higher TiO_2 concentrations and lower Zr/Nb. Moreover, ratios of highly incompatible elements often used as source indicators such as Nb/U, Ce/Pb, and Ba/Th, which are distinct between the groups, are not changed by varying degrees of melting of mantle consisting of olivine, orthopyroxene, clinopyroxene and garnet/spinel (e.g. Hofmann, 2014). This indicates that varying degrees of melting are not the primary cause for the differences between the groups. Instead, we interpret the geochemical trends to represent mixing between low K_2O-high Nb/U OIB-like asthenospheric melts and high K_2O-low Nb/U melts most likely derived from the lithospheric mantle. In the following, we will discuss how such high K_2O-low Nb/U melts could have been formed through either 1) percolative fractional crystallization of asthenospheric melts within the lithospheric mantle or 2) by re-melting of pyroxenitic/amphibolitic veins formed by the first mentioned process.

ACCEPTED MANUSCRIPT

Percolative fractional crystallization and melt-peridotite interaction during ascent

Melt-mantle interaction during percolation of the asthenospheric melts through the lithospheric mantle would lead to reactions similar to those found in the experiments performed by Lambert et al. (2012) which are generally representative for reaction experiments from the literature (e.g. Mallik and Dasgupta, 2012; Morgan and Liang, 2005; Wang et al., 2013). In these experiments, melts reacted with peridotite at 1.5 GPa pressure and 1250 °C temperature and at 2.5 GPa and 1400 °C which are conditions that are representative for the shallow and deeper lithospheric mantle, respectively. In one set of the experiments, weakly silica-undersaturated but rather silica-rich (50.6 wt.% SiO_2) melt was reacted with peridotite and this led to precipitation of mainly orthopyroxene (opx) at 1.5 GPa and mainly clinopyroxene (cpx) at 2.5 GPa while olivine in both cases was dissolved. In the experiments involving a more Si-undersaturated low-Si melt (41.6 wt.% SiO_2), opx was dissolved and olivine and mainly cpx precipitated. Due to consumption of melt by the interaction with sub-solidus peridotite in both experiments, the alkali and TiO_2 concentrations (and thus by inference all other incompatible trace elements) were increased in the melt (Lambert et al., 2012).

The plot in Fig. 10a shows the enrichment of three low Nb/U compositions (inclusion 4-128 from sample 124567, wr sample 126230 from Søager et al. (2013), and inclusion 5-33 from sample CL467) relative to high Nb/U inclusion 5-28 from sample CL467 which has low K_2O and high Nb/U and SiO_2. The low Nb/U compositions are in most cases ~2-5 times enriched in the most incompatible elements from Rb to Zr, including the light rare earth elements (LREE) and Cs (not shown), whereas the middle (MREE) and heavy REE (HREE) are at the same level as in the high Nb/U inclusion. If the enrichment was produced by melt-peridotite interaction alone, it would therefore require that more than 50 % of the melt was consumed in the reactions and that a crystallizing phase retained part of the MREEs and HREEs to prevent them from being enriched in the melt. Both olivine, opx, and amphibole in basaltic systems have partition coefficients for the M-HREEs below 1 (e.g. Frei et al., 2009; Ionov et al., 1997; Kennedy et al., 1993; LaTourrette et al., 1995) and are thus incapable of

ACCEPTED MANUSCRIPT

buffering the concentrations at a constant level. Garnet has partition coefficients for the M-HREEs above 1 and could retain these elements in the residue but would also increase Dy/Yb in the melt. Yet, the high K_2O, low Nb/U samples in many cases have lower Dy/Yb than the low K_2O, high Nb/U samples (Fig. 8f), so garnet cannot have played a role in their formation. In contrast, the absence of garnet at low pressures in the spinel stability field favors formation of cpx with a high Ca-Tschermak's component with partition coefficients for the M-HREEs around 1 that do not fractionate these elements (Blundy et al., 1998; Green et al., 2000; Hill et al., 2000; Lundstrom et al., 1998). In Fig. 10a, the black line shows the composition of inclusion 5-28 with 50 % cpx removed by fractional crystallization using mainly the low pressure partition coefficients from Green et al. (2000) (see figure caption 10). This model reproduces the REE patterns and the enrichment in the high field strength elements (HFSE) Zr, Hf, Nb and Ta in the most enriched low Nb/U melts relative to inclusion 5-28. This suggests that cpx plays an important role in the formation of the low Nb/U melts, as is also indicated by the lower CaO, MnO, Sc/Hf and V/Hf of the low Nb/U samples and inclusions which could have been produced by retention of the compatible CaO, MnO, Sc and V relative to the incompatible Hf in residual cpx. This could for example be through cpx crystallization during melt-peridotite interaction or by melting of cpx-rich lithologies. Since both lower and higher-Si alkaline melts can crystallize large amounts of cpx during melt-peridotite interaction at lithospheric mantle levels (Lambert et al., 2012), this is a viable hypothesis. In a more sophisticated model of melt-rock interaction as presented by Bedini et al. (1997), the simultaneous dissolution of olivine during crystallization of cpx dilutes the M-HREEs in the melt and therefore partition coefficients for these elements need not be as high as 1.

Harte et al. (1993) proposed that mantle melts may be modified by "percolative fractional crystallization" during passage through the lithospheric mantle. A porous flow of basaltic melt through the peridotitic mantle will result in melt-peridotite reactions including extensive crystallization of the melt, chromatographic reactions and equilibration with the peridotite and form veins and metasomatized mantle.

ACCEPTED MANUSCRIPT

Bedini et al. (1997) modeled the melt trace element development in this type of melt-rock reactions and showed that they lead to strong enrichments in the most incompatible elements in the residual melts, including U, La and the other LREEs, while the more compatible M-HREEs remain almost constant. In their model, crystallization of trace amounts of rutile caused Nb and Ta to also remain at a constant level thereby producing high La/Nb and low Nb/U melts. The Río Colorado low Nb/U basalts have the same range of La/Nb as the high Nb/U (Fig. 9e) and therefore, to explain the melt evolution from high to low Nb/U melt with this type of process requires co-crystallization of a mineral phase incorporating the LREEs, such as apatite, during the melt-rock reaction. Bedini et al. (1997) suggested that in the later stages of melt-rock reactions rutile and apatite crystallize from the melt in a ~0.25 ratio (rutile/apatite) together with cpx while opx is dissolved into the melt enriching the melt in SiO_2. To qualitatively estimate the effect of such a crystallization on the trace element patterns, we removed 70 % crystals (94 % cpx, 4 % apatite and 1 % rutile) by fractional crystallization from the high Nb/U inclusion 5-28 (Fig. 10a). Partition coefficients for Nb and Ta in rutile were arbitrarily set to 30 for both elements. These partition coefficients vary considerably in the literature but most studies find $D_{Nb}/D_{Ta} < 1$ (Klemme et al., 2005; Xiong et al., 2005 and references herein) which would result in increased Nb/Ta in the melts. We note that the Nb/Ta ratios of the low Nb/U basalts are very similar to the high Nb/U basalts and this argues against the involvement of rutile. However, some studies have found $D_{Nb}/D_{Ta} > 1$ (e.g. Foley et al., 2000) and metasomatic rutile with near-chondritic Nb/Ta (Bodinier et al., 1996) so fractional crystallization of rutile cannot be ruled out entirely. The much lower partition coefficients for Nb and Ta in ilmenite and titanite (e.g. Klemme et al., 2006; Prowatke and Klemme, 2005) would require unrealistically large proportions of fractionation of these minerals which would quickly deplete the melts in TiO_2.

Despite the fact that this is an oversimplified approach which does not account for the chromatographic effects and dissolution of mantle minerals, the modeled composition shows that reactions involving fractionation of the suggested minerals could potentially produce the overall enrichment pattern of

ACCEPTED MANUSCRIPT

the low Nb/U basalts and most of the observed changes in the trace element ratios (black lines in Fig. 9). The chromatographic effect adds highly incompatible elements from the mantle to the melts causing a much stronger enrichment in incompatible elements (Bedini et al., 1997) which may be enhanced by leaching of fluid-mobile elements from the wall rocks by the fluid-rich residual melts. Such processes may explain the excessive enrichment in mainly Cs, Rb, Th and U relative to the model in Fig. 10. We consider melt-rock reactions within the lithospheric mantle similar to those proposed by Harte et al. (1993) and Bedini et al. (1997) as a possible model for generating low amounts of highly enriched low Nb/U melt that could subsequently mix with new batches of high Nb/U melt.

Vein melting in the lithospheric mantle

In contrast to the above described model, where the low Nb/U component represents the evolved melts after melt-rock interaction, Pilet and co-workers developed a model for generation of intraplate basanites by re-melting of veins produced by the melt-rock reactions (Pilet et al., 2005, 2008, 2011, 2015). In this section we will evaluate whether re-melting of metasomatized and veined mantle could be an alternative model for formation of the low Nb/U melts.

The low Nb/U mixing component is very similar to compositions of alkaline lamprohyres, such as camptonites and monchiquites, both in major and trace elements (Fig. 10b and 11). These rocks range from transitional to moderately silica-undersaturated compositions, they have high Al_2O_3-contents, low to moderate K_2O-contents and K_2O/Na_2O (0.1–3.4 in the dataset shown in Fig. 10 and 11 and ~0.5 in most low Nb basalts) and negative or no K-anomalies (Fig. 10b). Le Maître (2002) defined camptonites and monchiquites as a variety of lamprophyres composed of phenocrysts of olivine, kaersutite, titanian augite, and Ti-rich biotite in a matrix of the same minerals (minus olivine) with plagioclase and subordinate alkali feldspar or feldspathoids.

ACCEPTED MANUSCRIPT

According to Mitchell (1994) and Bédard (1994), alkaline lamprophyres are alkali basalts that crystallized at elevated volatile pressures and typically were emplaced as dykes or sills. Therefore, the high K_2O-low Nb/U melt mixing end-member could be an equivalent to alkaline lamprohyres.

The suggested important role for cpx in the formation of the low Nb/U basalts could also be as a residual phase during melting if the source was pyroxenitic veins or pyroxene-rich metasomatized parts of the lithospheric mantle, as this would have a very similar effect on the trace element patterns as fractional crystallization of cpx. The wr low Nb/U samples generally have higher SiO_2, K_2O, Na_2O, Al_2O_3/TiO_2 and Na_2O/TiO_2 and lower TiO_2, FeO^T, CaO and CaO/Al_2O_3 than the high Nb/U basalts while most of the low Nb/U inclusions are shifted towards lower SiO_2, Na_2O, Al_2O_3/TiO_2 and Na_2O/TiO_2 but higher CaO and CaO/Al_2O_3 (Fig. 11). These compositions overlap and follow the trends outlined by the alkaline lamprophyres (Fig. 11) which have higher Na_2O and TiO_2 and in many cases lower SiO_2 and Al_2O_3/TiO_2 at a given Na_2O/TiO_2 than both lamproiites and melts of experimental unmetasomatized peridotite (see references in Fig. caption 11). The geochemical dissimilarities underline the generic difference between the lamproiites and alkaline lamprophyres that could be related to different types of mantle metasomatism.

Assuming that the end-member compositions for these trends represent melts of metasomatized mantle, we identify possible source lithologies which could generate the major element compositions of these melts. The experimental melt compositions that form the best match as the low SiO_2-low Na_2O/TiO_2 melt end-member are cpx -hornblendite melts formed at 1.5 GPa (Pilet et al., 2008). The pure hornblendite melts from Pilet et al. (2008) have very low SiO_2 (<39 wt.%) and high TiO_2 (>5.4 wt.%) and they can only have played a role in the genesis of alkaline lamprophyres if they were subsequently mixed with a higher SiO_2-higher Na_2O/TiO_2 melt or if they reacted with peridotite as suggested by van der Meer et al. (2017). The best match for the high SiO_2-high Na_2O/TiO_2 component could be peridotite melts formed at low pressures. In both pyroxenite and

ACCEPTED MANUSCRIPT

peridotite melts, only melts formed at low pressures (<~2 GPa) have sufficiently high SiO_2 and Na_2O/TiO_2 combined with low CaO/Al_2O_3 to generate the high- SiO_2-high Na_2O/TiO_2 magmas due to the inverse pressure dependencies of the partition coefficients for Na and Ti in cpx and the retention of Al in garnet at higher pressures yielding higher CaO/Al_2O_3 (e.g. Blundy et al. 1995; Hirschmann et al., 1999; Walter, 1998). Any suitable peridotitic source would need to have been refertilized by melts and/or fluids as in the starting compositions of the experiments by Kogiso et al. (1998) and Condamine and Médard (2014) to produce melts with sufficiently high Na_2O and K_2O (Fig. 11a and e). A second possibility is low degree pyroxenite melts, here represented by melts formed at 1.5 GPa by 3-13.5 % melting of a Si-undersaturated but hyperstene-normative garnet websterite representing the mean composition of naturally occurring pyroxenites (Lambert et al, 2009). Both a pyroxenitic and a peridotitic source would likely have been phlogopite-bearing to produce sufficiently K_2O-rich melts, like the phlogopite-lherzolite used in the experiments by Condamine and Médard (2014). It is not possible to confidently distinguish between mixing with peridotite and pyroxenite melts based on major element variations.

Highly Si-undersaturated pyroxenite melts may also contribute to alkaline lamprophyre magmas but the shown experimental melts in Fig. 11 (Hirschmann et al., 2003; Keshav et al., 2004; Lambert et al., 2009) do not have sufficiently high TiO_2 and low Al_2O_3/TiO_2 and Na_2O/TiO_2 to work as the low SiO_2-low Na_2O/TiO_2 end-member and such melts are probably less important in the genesis of alkaline lamprophyres. Direct melts of silica-rich eclogites (e.g. Pertermann and Hirschmann, 2003; Spandler et al., 2008) (not shown) are too SiO_2-rich and Mg-numbers are too low to be parental to the alkaline lamprophyres and low Nb/U rocks. Therefore, in terms of major element compositions, the low Nb/U and alkaline lamprophyre melts can have been formed at low pressures by melting of metasomatized peridotite and pyroxenite/amphibole pyroxenite veins in the lithospheric mantle. Pilet et al., (2005, 2011) argued that the Nb-rich melts dominating the alkaline ocean island basalts and intraplate basanites (e.g. sample 31 from Pilet et al. 2005, orange line in Fig. 10b) were

ACCEPTED MANUSCRIPT

produced by melting of veins formed at an intermediate stage of the percolative fractional crystallization in the phase where rutile, apatite and other minor phases crystallized along with amphibole and cpx, and that these minor phases were subsequently incorporated into the melts. This melt type is likely to dominate the low SiO_2-low Na_2O/TiO_2 lamprophyres whereas the low Nb/U inclusions with low SiO_2 do not have trace element patterns indicating melt-out of rutile and apatite (for example high Nb, Ta and LREE like the high-Nb basanite from Pilet et al., 2005, orange line in Fig. 10b) although the lowest SiO_2 –highest TiO_2 inclusion 5-33 does have higher Nb/U than the other low Nb/U inclusions (Nb/U = 47). The distinct major element compositions of the low Nb/U inclusions relative to the wr low Nb/U basalts may be due to simply the presence of amphibole in their source. The trace element patterns of the low Nb/U melts must represent mixing of high Nb/U melts with either the final liquids after crystallization of a.o. rutile and apatite or alternatively, re-melting of mantle metasomatized by these final fluid-rich melts. It is noteworthy that in comparison to the highly alkaline high Nb/U basanites from Pilet et al. (2005), the Río Colorado high Nb/U basalts are only weakly Si-undersaturated and far less enriched (Fig. 10b) supporting the suggestion that they are asthenospheric melts formed at higher degrees of melting.

To model the mixing between asthenospheric and lithospheric mantle melts, we calculated simple mixing lines shown in Fig. 11 between fractionation corrected high Nb/U compositions and various experimental melts. To model the inclusions, high Nb/U inclusion 5-28 from sample CL467 was mixed with the cpx -hornblendite melt AG7-4 (54 % melting, Pilet et al., 2008) (lines with crosses in Fig. 11). For the wr Nb/U basalts, sample 124564 was mixed with either the phlogopite lherzolite melt sta17 (19% melting, Condamine and Médard, 2014) (lines with small bars) or the pyroxenite melt 40-E2 (13.5 % melting, Lambert et al., 2009) (lines with asterisks). The best fits to the most enriched inclusions and low Nb/U samples suggest that up to 30-50 % enriched lithospheric mantle melt mixed with the asthenospheric high Nb/U melts.

ACCEPTED MANUSCRIPT

Generic model for the low Nb/U basalts

The evidence presented above suggests that the low Nb/U magmas contain melts of lithospheric mantle metasomatized and veined by melt and fluids from the asthenospheric Río Colorado source. The metasomatism and veining may have happened during the earlier episodes of similar volcanism in the area, either during the large scale early Miocene Matancilla-Fortunoso volcanism (Dyhr et al., 2013a and b; Kay and Copeland, 2006), the smaller scale Pliocene volcanism (Kay et al., 2013) or the early Pleistocene volcanism in the Auca Mahuida volcanic field just south of Río Colorado (Kay et al., 2006b, 2013). All of these basalts have elemental and isotopic compositions very similar to the Río Colorado basalts (Fig. 2) (Dyhr et al., 2013a and b; Kay et al., 2013; Søager and Holm, 2013). At the early stages of volcanism, asthenospheric melts crystallized when cooled in the lithospheric mantle (McKenzie, 1989) and metasomatized the mantle around the melt conduits. During the more intensive phase of volcanism in the Río Colorado volcanic field, the enhanced high Nb/U volcanism increased the temperature of the lithospheric mantle locally. This enabled the asthenospheric magmas to melt the metasomatized regions leading to eruption of asthenospheric magmas mixed with smaller or larger amounts of low Nb/U-high-K_2O melts from the lithospheric mantle. The melting may also have been partly triggered by tectonic movements in the lithosphere which was tectonically active during the Pleistocene (Rosello et al., 2002).

The lithospheric mantle in the Río Colorado region is dominated by anhydrous spinel lherzolites with only minor harzburgite and pyroxenite (Bertotto et al., 2013, Jalowitzki et al., 2010). According to Jalowitzki et al. (2010) and Bertotto et al. (2013), the lithospheric mantle is moderately depleted but experienced minor metasomatism by subduction zone fluids and melts. The $^{87}Sr/^{86}Sr$ isotopic compositions of the mantle xenoliths (n = 12) range from 0.702874 to 0.704999 with an average of 0.704035 (Jalowitzki et al., 2010) and thus, they

ACCEPTED MANUSCRIPT

often have higher values than the Río Colorado basalts (0.7035-0.7039) but the contrast is minor. The $^{143}Nd/^{144}Nd$ isotopic compositions of three mantle xenoliths range from 0.51284 to 0.51342 (Jalowitzki et al., 2010) and again overlap the isotopic range of the Río Colorado basalts (0.51287-0.51279). Therefore, contributions of Sr and Nd from the lithospheric mantle to the melts may not be easily detectable, but could cause $^{87}Sr/^{86}Sr$ to increase. However, the Sr concentrations in the xenoliths are in all cases below 7 ppm whereas the high Nb/U basalts have ~600-700 ppm. Consequently, any veins of high Nb/U material and surrounding metasomatized mantle would be overwhelmed with Sr from the intruding melt, and the lithospheric mantle would not convey a significant imprint to the isotopic composition of the later formed low Nb/U melts.

The concept of re-melting veins and metasomatized parts of the lithospheric mantle formed by plume melts in the earlier phases of the same volcanic episode has also been suggested elsewhere. For example in Damaraland, Namibia, where le Roex and Lanyon (1998) suggested that the lamprophyre and carbonatite intrusions were melts of metasomatic vein material emplaced by the coeval Tristan plume volcanism. On the Tubuai and Canary Islands, Caroff et al. (1997) and Lundstrom et al. (2003), respectively, found that due to gradual heating of the lithosphere by plume melts, the magmas of the later stages of volcanism incorporated melts of both the peridotite and of pyroxene or amphibole-bearing veins in the lithospheric mantle formed during the initial volcanic stages. It is therefore important to bear in mind when interpreting intraplate rocks that they can be mixtures of melts from asthenospheric and lithospheric sources despite the fact that they have similar isotopic compositions.

ACCEPTED MANUSCRIPT

Conclusions

The Río Colorado high K_2O-low Nb/U melt components have similar origins as alkaline lamprophyric rocks. They are presumably derived by mixing of high Nb/U melts with either 1) fluid-rich residual melts after extensive percolative fractional crystallization of high Nb/U melts in the lithospheric mantle involving fractionation of clinopyroxene, apatite and rutile or 2) melts of phlogopite-bearing pyroxenite veins (±amphibole) and metasomatized peridotitic lithospheric mantle formed/metasomatized by residual melts after percolative fractional crystallization involving fractionation of apatite and rutile. We propose that the lithospheric mantle was metasomatized and veined by melts from the upwelling Río Colorado asthenospheric mantle in the earlier periods of volcanism in the area. The metasomatized mantle was later re-melted during the continued volcanic activity forming the Río Colorado volcanic field and the resulting high K_2O, low Nb/U melts mixed in different proportions with asthenospheric low K_2O, high Nb/U melts.

Acknowledgements

Christina Bonanati is thanked for assistance and company during field work. We greatly acknowledge the help of Mario Thöner and Ulrike Westerströer in the analytical work. Heidi Wehrmann and Guillaume Jacques are thanked for their practical assistance and good discussions. We thank the reviewers, Vadim Kamenetsky and Simon Matthews, for good comments that helped to improve the manuscript.

ACCEPTED MANUSCRIPT

ACCEPTED MANUSCRIPT

Funding

This work was supported by the Danish Council for Independent Research, Natural Sciences [grant no. 0602-02528B to N.S.] and the GEOMAR Helmholtz Center for Ocean Sciences Kiel.

References

Aghazadeh, M., Prelević, D., Badrzadeh, Z., Braschi, E., van den Bogaard, P., Conticelli, S., 2015. Geochemistry, Sr–Nd–Pb isotopes and geochronology of amphibole- and mica-bearing lamprophyres in northwestern Iran: Implications for mantle wedge heterogeneity in a palaeo-subduction zone. Lithos 216-217:352-369

Batki, A., Pál-Molnár, E., Dobosi, G., Skelton, A., 2014. Petrogenetic significance of ocellar camptonite dykes in the Ditrău Alkaline Massif, Romania. Lithos 200-201, 181-196

Bayat, F., Torabi, G., 2011. Alkaline lamprophyric province of Central Iran. Island Arc 20, 386-400

Bédard, J.H., 1994. Mesozoic east North American alkaline magmatism: Part 1. Evolution of Monteregian lamprophyres, Québec, Canada. Geochimica et Cosmochimica Acta 58, 95-112

Bedini, R.M., Bodinier, J.-L., Dautria, J.-M., Morten, L., 1997. Evolution of LILE-enriched small melt fractions in the lithospheric mantle: a case study from the East African Rift. Earth and Planetary Science Letters 153, 67-83.

Bermudez, A., Delpino, D., Frey, F., Saal, A., 1993. Los basaltos de retroarco extraandinos, in: Ramos, V.A. (Eds.), Geología y Recursos Naturales de Mendoza. Relatorio I(13), pp. 161-172.

Bertotto, G.W., Orihashi, Y., Nagao, K., Motoki, A., 2006. New K-Ar ages on retroarc basalts of Mendoza-La Pampa. Abstract, Segundo Encuentro Cientifico ICES Nov 2006, Buenos Aires.

ACCEPTED MANUSCRIPT

Bertotto, G.W., Cingolani, C.A., Bjerg, E.A., 2009. Geochemical variations in Cenozoic backarc basalts at the border of La Pampa and Mendoza provinces, Argentina. Journal of South American Earth Sciences 28, 360-373.

Bertotto, G.W., Mazzucchelli, M., Zanetti, A., Vannucci, R., 2013. Petrology and geochemistry of the back-arc lithospheric mantle beneath eastern Payunia (La Pampa, Argentina): Evidence from Agua Poca peridotite xenoliths. Geochemical Journal 47, 219-234.

Blundy, J.D., Falloon, T.J., Wood, B.J., Dalton, J.A., 1995. Sodium partitioning between clinopyroxene and silicate melts. Journal of Geophysical Research 100, B8, 15,501-15,515.

Blundy, J.D., Robinson, J.A.C., Wood, B.J., 1998. Heavy REE are compatible in clinopyroxene on the spinel lherzolite solidus. Earth and Planetary Science Letters 160, 493–504.

Bodinier, J.-L., Merlet, C., Bedini, R.M., Simien, F., Remaidi, M., Garrido, C.J., 1996. Distribution of niobium, tantalum, and other highly incompatible trace elements in the lithospheric mantle: The spinel paradox. Geochimica et Cosmochimica Acta 60, 3, 545-550.

Borisov, A.A., Shapkin, A.I., 1990. A new empirical equation rating Fe^{3+}/Fe^{2+} in magmas to their composition, oxygen fugacity, and temperature. Geochemistry International 27, 111-116.

Burd, A.I., Booker, J.R., Mackie, R., Favetto, A., Pomposiello, M.C., 2014. Three-dimensional electrical conductivity in the mantle beneath the Payún Matrú Volcanic Field in the Andean backarc of Argentina near 36.5°S: evidence for decapitation of a mantle plume by resurgent upper mantle shear during slab steepening. Geophysical Journal International 198, 812-827.

Caroff, M., Maury, R.C., Guille, G., Cotton, J., 1997. Partial melting below Tubuai (Austral Islands, French Polynesia). Contributions to Mineralogy and Petrology 127, 369-382.

Class, C., Goldstein, S.L., 1997. Plume lithosphere interaction in the ocean basins: constraints from the source mineralogy. Earth and Planetary Science Letters 150, 245–260.

ACCEPTED MANUSCRIPT

Condamine, P., Médard, E., 2014. Experimental melting of phlogopite-bearing mantle at 1GPa: Implications for potassic magmatism. Earth and Planetary Science Letters 397, 80-92.

Danyushevsky, L.V., 2001. The effect of small amounts of H_2O on crystallization of mid-ocean ridge and backarc basin magmas. Journal of Volcanology and Geothermal Research 110, 265–280.

Danyushevsky, L.V., Della-Pasqua, F.N., Sokolov, S., 2000. Re-equilibration of melt inclusions trapped by magnesian olivine phenocrysts from subduction-related magmas: petrological implications. Contributions to Mineralogy and Petrology 138, 68–83.

Danyushevsky, L.V., Sokolov, S., Falloon, T.J., 2002. Melt inclusions in olivine phenocrysts: using diffusive re-equilibration to determine the cooling history of a crystal, with implications for the origin of olivine-phyric volcanic rocks. Journal of Petrology 43(9), 1651-1671.

Danyushevsky, L.V., Plechov, P., 2011. Petrolog3: Integrated software for modeling crystallization processes. Geochemistry Geophysics Geosystems 12, Q07021.

Dostal, J., Owen, J.V., 1998. Cretaceous alkaline lamprophyres from northeastern Czech Republic: geochemistry and petrogenesis. Geologischer Rundschau 87, 67-77.

Dyhr, C.T., Holm, P.M., Llambías, E.J., Scherstén, A., 2013a. Subduction controls on Miocene backarc lavas from Sierra de Huantraico and La Matancilla and new $^{40}Ar/^{39}Ar$ dating from the Mendoza region, Argentina. Lithos 179, 67-83.

Dyhr, C.T., Holm, P.M., Llambías, E.J., 2013b. Geochemical constraints on the relationship between the Miocene-Pliocene volcanism and tectonics in the Palaoco and Fortunoso volcanic fields, Mendoza Region, Argentina: New insights from $^{40}Ar/^{39}Ar$ dating, Sr-Nd-Pb isotopes and trace elements. Journal of Volcanology and Geothermal Research 266, 50-68.

Espanon, V.R., Honda, M., Chivas, A.R., 2014. Cosmogenic ^{3}He ^{21}Ne surface exposure dating of young basalts from southern Mendoza, Argentina. Quaternary Geochronology 19, 76-86.

ACCEPTED MANUSCRIPT

Foley, S.F., 1992a. Petrological characterization of the source components of potassic magmas: geochemical and experimental constraints. Lithos 28, 187–204.

Foley, S.F., 1992b. Vein-plus-wall-rock melting mechanisms in the lithosphere and the origin of potassic alkaline magmas. Lithos 28, 435–453.

Foley, S.F., Barth, M.G., Jenner, G.A., 2000. Rutile/melt partition coefficients for trace elements and an assessment of the influence of rutile on the trace element characteristics of subduction zone magmas. Geochimica et Cosmochimica Acta 64, 5, 933-938.

Folguera, A., Bottesi, G., Zapata, T., Ramos, V.A., 2008. Crustal collapse in the Andean backarc since 2 Ma: Tromen volcanic plateau, Southern Central Andes (36°40'-37°30'S). Tectonophysics 459, 140-160.

Folguera, A., Naranjo, J.A., Orihashi, Y., Sumino, H., Nagao, K., Polanco, E., Ramos, V.A., 2009. Retroarc volcanism in the northern San Rafael block (34°-35°30'S), southern Central Andes: Occurrence, age and tectonic setting. Journal of Volcanology and Geothermal Research 186, 169-185.

Frei, D., Liebscher, A., Franz, G., Wunder, B., Klemme, S., Blundy, J., 2009. Trace element partitioning between orthopyroxene and anhydrous silicate melt on the lherzolite solidus from 1.1 to 3.2 GPa and 1,230 to 1,535 °C in the model system Na_2O–CaO–MgO–Al_2O_3–SiO_2. Contributions to Mineralogy and Petrology 157, 473-490.

Gaetani, G.A., Kent, A.J.R., Grove, T.L., Hutcheon, I.D., Stolper, E.M., 2003. Mineral/melt partitioning of trace elements during hydrous peridotite partial melting. Contributions to Mineralogy and Petrology 145, 391-405.

Germa, A., Quidelleur, X., Gillot, P.Y., Tchilinguirian, P., 2010. Volcanic evolution of the backarc Pleistocene Payún Matrú volcanic field (Argentina). Journal of South American Earth Sciences 29, 717-730.

Gilbert, H., Beck, S., Zandt, G., 2006. Lithospheric and upper mantle structure of central Chile and Argentina. Geophysical Journal International 165, 383-398.

ACCEPTED MANUSCRIPT

Green, T.H., Blundy, J.D., Adam, J., Yaxley, G.M., 2000. SIMS determination of trace element partition coefficients between garnet, clinopyroxene and hydrous basaltic liquids at 2–7.5 GPa and 1080–1200°C. Lithos 53, 165-187.

Gudnason, J., Holm, P.M., Søager, N., Llambías, E.J., 2012. Geochronology of the late Pliocene to recent volcanic activity in the Payenia back-arc volcanic province, Mendoza, Argentina. Journal of South American Earth Sciences 37, 191-201.

Gurenko, A.A., Chaussidona, M., 1995. Enriched and depleted primitive melts included in olivine from Icelandic tholeiites: origin by continuous melting of a single mantle column. Geochimica et Cosmochimica Acta 59, 2905–2917.

Harangi, S., Tonarini, S., Vaselli, O., Manetti, P., 2003. Geochemistry and petrogenesis of Early Cretaceous alkaline igneous rocks in Central Europe: implications for a long-lived EAR-type mantle component beneath Europe. Acta Geologica Hungaria 46, 1, 77-94.

Harte, B., Hunter, R.H., Kinny, P.D., 1993. Melt geometry, movement and crystallization, in relation to mantle dykes, veins and metasomatism. Philosophical Transactions of the Royal Society of London A 342, 1-21.

Hier-Majumder, S., Anderson, I.M., Kohlstedt, D.L., 2005. Influence of protons on Fe–Mg interdiffusion in olivine. Journal of Geophysical Research 110, doi:10.1029/2004JB003292.

Hill, E., Wood, B.J., Blundy, J.D., 2000. The effect of Ca–Tschermaks component on trace element partitioning between clinopyroxene and silicate melt. Lithos 53, 205–217.

Hirose, K., Kushiro, I., 1993. Partial melting of dry peridotites at high pressures: Determination of compositions of melts segregated from peridotite using aggregates of diamond. Earth and Planetary Science Letters 114, 477-489.

Hirschmann, M.M., Ghiorso, M.S., Stolper, E.M., 1999. Calculation of peridotite partial melting from thermodynamic models of minerals and melts. II. Isobaric variations in melts near the solidus and owing to variable source composition. Journal of Petrology 40, 2, 297-313.

ACCEPTED MANUSCRIPT

Hirschmann, M.M., Kogiso, T., Baker, M.B., Stolper, E.M., 2003. Alkalic magmas generated by partial melting of garnet pyroxenite. Geology 31, 481-484.

Hofmann, A.W., 2014. Sampling mantle heterogeneity through oceanic basalts: isotopes and trace elements. Treatise of Geochemistry 2nd edition, vol. 3, 67-101.

Holm, P.M., Søager, N., Alfastsen, M., Bertotto, G.W., 2016. Subduction zone mantle enrichment by fluids and Zr–Hf-depleted crustal melts as indicated by backarc basalts of the Southern Volcanic Zone, Argentina. Lithos 262, 135-152.

Ionov, D.A., Griffin, W.L., O'Reilly, S.Y., 1997. Volatile-bearing minerals and lithophile trace elements in the upper mantle. Chemical Geology 141, 153-184.

Jacques, G., Hoernle, K., Gill, J., Hauff, F., Wehrmann, H., Garbe-Schönberg, D., van den Bogaard, P., Bindeman, I., Lara, L.E., 2013. Across-arc geochemical variations in the Southern Volcanic Zone, Chile (34.5-38.0°S): Constraints on mantle wedge and slab input compositions. Geochimica et Cosmochimica Acta 123, 218-243.

Jalowitzki, T.L.R., Conceição, R.V., Orihashi, Y., Bertotto, G.W., Nakai, S., Schilling, M.E., 2010. Evolução geoquímica de peridotitos e piroxenitos do Manto Litosférico Subcontinental do vulcão Agua Poca, Terreno Cuyania, Argentina. Pesquisas em Geociências 37, 2, 143-167.

Jarosewich, E.J., Nelen, J.A., Norberg, J.A., 1980. Reference samples for electron microprobe analysis. Geostandards Newsletters 4, 43-47.

Jochum, K.P., Stoll, B., Herwig, K., Willbold, M., Hofmann, A.W., Amini, M., Aarburg, S., Abouchami, W., Hellebrand, E., Mocek, B., Raczek, I., Stracke, A., Alard, O., Bouman, C., Becker, S., Dücking, M., Brätz, H., Klemd, R., de Bruin, D., Canil, D., Cornell, D., de Hoog, C.-J., Dalpé, C., Danyushevsky, L., Eisenhauer, A., Gao, Y., Snow, J.E., Groschopf, N., Günther, D., Latkoczy, C., Guillong, M., Hauri, E.H., Höfer, H.E., Lahaye, Y., Horz, K., Jacob, D.E., Kasemann, S.A., Kent, A.J.R., Ludwig, T., Zack, T., Mason, P.R.D., Meixner, A., Rosner, M., Misawa, K., Nash, B.P., Pfänder, J., Premo, W.R., Sun, W.D., Tiepolo, M., Vannucci, R., Vennemann, T., Wayne, D., Woodhead, J.D., 2006. MPI-DING reference glasses for in situ microanalysis: New reference values for element concentrations and isotope ratios. Geochemistry Geophysics Geosystems 7, 2, doi:10.1029/2005GC001060.

ACCEPTED MANUSCRIPT

Jochum, K.P., Weis, U., Stoll, B., Kuzmin, D., Yang, Q., Raczek, I., Jacob, D.E., Stracke, A., Birbaum, K., Frick, D.A., Günther, D., Enzweiler, J., 2011. Determination of Reference Values for NIST SRM 610—617 Glasses Following ISO Guidelines. Geostandards and Geoanalytical Research 35, 4, 397-429.

Kay, S.M., Gorring, M., Ramos, V.A., 2004. Magmatic sources, setting, and causes of Eocene to Recent Patagonian plateau magmatism (36 degrees S to 52 degrees S latitude). Revista de la Asociación Geologica de Argentina 59, 4, 556-568.

Kay, S.M., Burns, W.M., Copeland, P., Mancilla, O., 2006a. Upper Cretaceous to Holocene magmatism and evidence for transient Miocene shallowing of the Andean subduction zone under the northern Neuquén Basin. Geological Society of America Special Paper 407, 19-60.

Kay, S.M., Copeland, P., 2006. Early to middle Miocene backarc magmas of the Neuquén basin: Geochemical consequences of slab shallowing and the westward drift of South America. Geological Society of America Special Paper 407, 185-213

Kay, S.M., Copeland, P., Mancilla, O., 2006b. Evolution of the late Miocene Chachahuén volcanic complex at 37 ˚S over a transient shallow subduction zone under the Neuquén Andes. Geological Society of America Special Paper 407, 215-246.

Kay, S.M., Jones, H.A., Kay, R.W., 2013. Origin of Tertiary to Recent EM- and subduction-like chemical and isotopic signatures in Auca Mahuida region (37-38°S) and other Patagonian plateau lavas. Contributions to Mineralogy and Petrology 166, 1, 165-192.

Kendrick, E., Bevis, M., Smalley, Jr.R., Brooks, B., Vargas, R.B., Lauria, E., Souto, L.P., 2003. The Nazca-South America Euler vector and its rate of change. Journal of South American Earth Sciences 16, 125–131.

Kennedy, A.K., Lofgren, G.E., Wasserburg, G.J., 1993. An experimental study of trace element partitioning between olivine, orthopyroxene and melt in chondrules: equilibrium values and kinetic effects. Earth and Planetary Science Letters 115, 177–195.

Keshav, S., Gudfinnsson, G.H., Sen, G., Fei, Y., 2004. High-pressure melting experiments on garnet clinopyroxenite and the alkalic to tholeiitic transition in ocean-island basalts. Earth and Planetary Science Letters 223, 365-379.

ACCEPTED MANUSCRIPT

Klemme, S., Prowatke, S., Hametner, K, Günther, D., 2005. Partitioning of trace elements between rutile and silicate melts: Implications for subduction zones. Geochimica et Cosmochimica Acta 69, 9, 2361–2371.

Klemme, S., Günther, D., Hametner, K., Prowatke, S., Zack, T., 2006. The partitioning of trace elements between ilmenite, ulvospinel, armalcolite and silicate melts with implications for the early differentiation of the moon. Chemical Geology 234, 251-263.

Kogiso, T., Hirose, K., Takahashi, E., 1998. Melting experiments on homogeneous mixtures of peridotite and basalt: application to the genesis of ocean island basalts. Earth and Planetary Science Letters 162, 45-61.

Kogiso, T., Hirschmann, M.M., 2006. Partial melting experiments of bimineralic eclogite and the role of recycled mafic oceanic crust in the genesis of ocean island basalts. Earth and Planetary Science Letters 249, 188-199.

Lambert, S., Laporte, D., Schiano, P., 2009. An experimental study of pyroxenite partial melts at 1 and 1.5 GPa: Implications for the major-element composition of Mid-Ocean Ridge Basalts. Earth and Planetary Science Letters 288, 335-347.

Lambert, S., Laporte, D., Provost, A., Schiano, P., 2012. Fate of pyroxenite-derived melts in the peridotitic mantle: Thermodynamic and experimental constraints. Journal of Petrology 53, 3, 451-476.

LaTourrette, T., Hervig, R.L., Holloway, J.R., 1995. Trace element partitioning between amphibole, phlogopite, and basanite melt. Earth and Planetary Science Letters 135, 13-30.

Le Maître, R.W., 2002. Igneous Rocks: A Classification and Glossary of Terms: Recommendations of the International Union of Geological Sciences Subcommission on the Systematics of Igneous Rocks. Cambridge University Press, Cambridge, 236 pp.

Le Roex, A.P., Lanyon, R., 1998. Isotope and trace element geochemistry of Cretaceous Damaraland lamprophyres and carbonatites, Northwestern Namibia: evidence for plume–lithosphere interactions. Journal of Petrology 39, 6, 1117-1146.

ACCEPTED MANUSCRIPT

Lundstrom, C.C., Shaw, H.F., Ryerson, F.J., Williams, Q., Gill, J., 1998. Crystal chemical control of clinopyroxene–melt partitioning in the Di–Ab–An system: implications for elemental fractionations in the depleted mantle. Geochimica et Cosmochimica Acta 62, 2849–2862.

Lundstrom, C.C., Hoernle, K.A., Gill, J., 2003. U-series disequilibria in volcanic rocks from the Canary Islands: plume versus lithospheric melting. Geochimica et Cosmochimica Acta 67, 4153–4177.

Maaløe, S., 2011. Olivine Phenocryst Growth in Hawaiian Tholeiites: Evidence for Supercooling. Journal of Petrology 52, 7-8, 1579-1589.

Mallik, A., Dasgupta, R., 2012. Reaction between MORB-eclogite derived melts and fertile peridotite and generation of ocean island basalts. Earth and Planetary Science Letters 329-330, 97-108.

McDonough, W.F., Sun, S.-S., 1995. Composition of the earth. Chemical Geology 120, 223-253.

McKenzie, D., 1989. Some remarks on the movement of small melt fractions in the mantle. Earth and Planetary Science Letters 95, 53-72.

Mitchell, R.H., 1994. The lamprophyre facies. Mineralogy and Petrology 51, 137-146.

Morgan, Z., Liang,Y., 2005. An experimental study of the kinetics of lherzolite reactive dissolution with applications to melt channel formation. Contributions to Mineralogy and Petrology 150, 4, 369-385.

Orejana, D., Villaseca, C., Paterson, B.A., 2008. Geochemistry of pyroxenitic and hornblenditic xenoliths in alkaline lamprophyres from the Spanish Central System. Lithos 86, 167-96.

Pertermann, M., Hirschmann, M.M., 2003. Anhydrous partial melting experiments on MORB-like eclogite: phase relations, phase compositions and mineral–melt partitioning of major elements at 2–3 GPa. Journal of Petrology 44, 2173–2201.

ACCEPTED MANUSCRIPT

Pesicek, J.D., Engdahl, E.R., Thurber, C.H., DeShon, H.R., Lange, D., 2012. Mantle subducting slab structure in the region of the 2010M8.8 Maule earthquake (30–40°S), Chile. Geophysical Journal International 191, 317-324.

Pilet, S., Hernandez, J., Sylvester, P., 2005. The metasomatic alternative for ocean island basalt chemical heterogeneity. Earth and Planetary Science Letters 236, 148–166.

Pilet, S., Baker, M.B., Stolper, E.M., 2008. Metasomatized lithosphere and the origin of alkaline lavas. Science 320, 916–919.

Pilet, S., Baker, M.B., Münterner, O., Stolper, E.M., 2011. Monte Carlo simulations of metasomatic enrichment in the lithosphere and implications for the source of alkaline basalts. Journal of Petrology 52, 7-8, 1415-1442.

Pilet, S., 2015. Generation of low-silica alkaline lavas: Petrological constraints, models, and thermal implications. Geological Society of America Special Paper 514, 281-304.

Prelević, D., Foley, S.F., Romer, R.L., Cvetković, V., Downes, H., 2005. Tertiary ultrapotassic volcanism in Serbia: constraints on petrogenesis and mantle source characteristics. Journal of Petrology 46, 7, 1443-1487.

Prelević, D., Foley, S.F., Romer, R.L., Conticelli, S., 2008. Mediterranean Tertiary lamproites derived from multiple source components in postcollisional geodynamics. Geochimica et Cosmochimica Acta 72, 2125-2156.

Prowatke, S., Klemme, S., 2006. Trace element partitioning between apatite and silicate melts. Geochimica et Cosmochimica Acta 70, 4513–4527.

Qian, S.-P., Ren, Z.-Y., Zhang, L., Hong, L.B., Liu, J.-G., 2015. Chemical and Pb isotope composition of olivine-hosted melt inclusions from the Hannuoba basalts, North China Craton: Implications for petrogenesis and mantle source. Chemical Geology 401, 111-125.

Ramos, V.A., Folguera, A., 2011. Payenia volcanic province in the Southern Andes: An appraisal of an exceptional Quaternary tectonic setting. Journal of Volcanology and Geothermal Research 201, 1-4, 53-64.

ACCEPTED MANUSCRIPT

Ren, Z.Y., Ingle, S., Takahashi, E., Hirano, N., Hirata, T., 2005. The chemical structure of the Hawaiian mantle plume. Nature 436, 837–840.

Rock, N.M.S., 1991. Lamprophyres. Blackie and Son, Glasgow

Rosello, E.A., Cobbold, P.R., Diraison, M., Arnaud, N., 2002. Auca Mahuida (Neuquén Basin, Argentina): A Quarternary shield volcano on a hydro-carbon producing substrate. 5° International Symposium on Andean Geodynamics, Toulouse, extended abstracts, 549-552.

Rudnick, R.L., Gao, S., 2003. Composition of the continental crust, in: Carlson, R.W., Holland, H.D., Turekian, K.K. (Eds.), Treatise on Geochemistry: The Crust. Elsevier, pp. 1–64.

Salters, V.J.M., Longhi, J., 1999. Trace element partitioning during the initial stages of melting beneath mid-ocean ridges. Earth and Planetary Science Letters 166, 15-30.

Simonetti, A., Goldstein, S.L., Schmidberger, S.S., Viladkar, S.G., 1998. Geochemical and Nd, Pb, and Sr Isotope Data from Deccan Alkaline Complexes—Inferences for Mantle Sources and Plume–Lithosphere Interaction. Journal of Petrology 39, 11-12, 1847-1864.

Sobolev, A.V., Hofmann, A.W., Nikogosian, I.K., 2000. Recycled oceanic crust observed in 'ghost plagioclase' within the source of Mauna Loa lavas. Nature 404, 986–990.

Sobolev, A.V., Hofmann, A.W., Kuzmin, D.V., Yaxley, G.M., Arndt, N.A., Chung, S.-L., Danyushevsky, L.V., Elliott, T., Frey, F.A., Garcia, M.O., Gurenko, A.A., Kamenetsky, V.S., Kerr, A.C., Krivolutskaya, N.A., Matvienkov, V.V., Nikogosian, I.K., Rocholl, A., Sigurdsson, I.A., Sushchevskaya, N.M., Teklay, M., 2007. The amount of recycled crust in sources of mantle derived melts. Science 316, 412-417.

Sorbadere, F., Médard, E., Laporte, D., Schiano, P., 2013. Experimental melting of hydrous peridotite–pyroxenite mixed sources: Constraints on the genesis of silica-undersaturated magmas beneath volcanic arcs. Earth and Planetary Science Letters 384, 42-56.

ACCEPTED MANUSCRIPT

Spandler, C., Yaxley, G., Green, D.H., Rosenthal, A., 2008. Phase relations and melting of anhydrous K-bearing eclogite from 1200 to 1600˚C and 3 to 5 GPa. Journal of Petrology 49, 4, 771-795.

Søager, N., Holm, P.M., 2013. Melt-peridotite reactions in upwelling EM1-type eclogite bodies: constraints from alkaline basalts in Payenia, Argentina. Chemical Geology 360-361, 204-219.

Søager, N., Holm, P.M., Llambías, E.J., 2013. Payenia volcanic province, southern Mendoza, Argentina: OIB mantle upwelling in a backarc environment. Chemical Geology 349-350, 36-53.

Søager, N., Holm, P.M., Thirlwall, M.F., 2015a. Sr, Nd, Pb and Hf isotopic constraints on mantle sources and crustal contaminants in the Payenia volcanic province, Argentina. Lithos 212-215, 368-378.

Søager, N., Portnyagin, M., Hoernle, K., Holm, P.M., Hauff, F., Garbe-Schönberg, D., 2015b. Olivine major and trace element compositions in southern Payenia basalts, Argentina: evidence for pyroxenite-peridotite melt mixing in a backarc setting. Journal of Petrology 56, 8, 1495-1518.

Tappe, S., Foley, S.F., Jenner, G.A., Heaman, L.M., Kjarsgaard, B.A., Romer, R.L., Stracke, A., Joyce, N., Hoefs, J., 2006. Genesis of ultramafic lamprophyres and carbonatites at Aillik Bay, Labrador: a consequence of incipient lithospheric thinning beneath the North Atlantic craton. Journal of Petrology 47, 1261–1315.

Tassara, A., Götze, H.-J., Schmidt, S., Hackney, R., 2006. Three-dimensional density model of the Nazca plate and the Andean continental margin. Journal of Geophysical Research 111, B9.

van der Meer, Q.H.A., Waight, T.E., Scott, J.M., Münker, C., 2017. Variable sources for Cretaceous to recent HIMU and HIMU-like intraplate magmatism in New Zealand. Earth and Planetary Science Letters 469, 27-41.

Vergani, G.D., Tankard, A.J., Belotti, H.J., Welsink, H.J., 1995. Tectonic evolution and paleogeography of the Neuquén Basin Argentina, in: Tankard, A.J., Suárez, R., Welsink, H.J. (Eds.), Petroleum basins of South America. American Association of Petroleum Geology Mem 62, 383-402.

Walter, M.J., 1998. Melting of garnet peridotite and the origin of komatiite and depleted lithosphere. Journal of Petrology 39, 1, 29-60.

ACCEPTED MANUSCRIPT

Wang, C., Liang, Y., Xu, W., Dygert, N., 2013. Effect of melt composition on basalt and peridotite interaction: laboratory dissolution experiments with applications to mineral compositional variations in mantle xenoliths from the North China Craton. Contributions to Mineralogy and Petrology 166, 1469-1488.

Wass, S.Y., Rogers, N.W., 1980. Mantle metasomatism -precursor to continental alkaline volcanism. Geochimica et Cosmochimica Acta 44, 1811-1823.

Xiong, X.L., Adam, J., Green, T.H., 2005. Rutile stability and rutile/melt HFSE partitioning during partial melting of hydrous basalt: Implications for TTG genesis. Chemical Geology 218, 339-359.

Figure captions

Fig. 1. a) A map of the southern part of South America with the Payenia province as shown in b) marked with a square. CT is the Chile Trench (dotted line), CR is the Chile rise. b) An overview map of the Payenia province (outlined with a dashed line). The square marks the area of the image shown in c. The dotted line shows the Chile-Argentina border. The black triangles mark the volcanoes of the present day arc front of the Southern Volcanic Zone. c) A satellite image from Google Earth Pro showing the sampled cones and the sample localities with yellow markers

Fig. 2. a) $^{87}Sr/^{86}Sr$ vs. $^{206}Pb/^{204}Pb$, b) Th/La vs. Nb/U of whole rocks from the Payenia province and the SVZ arc. The high and low Nb/U rocks have overlapping isotopic compositions but distinct trace element compositions. The fields for C +TSVZ arc show data from the Central and Transitional Southern Volcanic Zone arc. Data is from Holm et al. (2014), Kay et al. (2004, 2013), Jacques et al. (2013), Søager and Holm (2013) and Søager et al. (2013, 2015a, 2015b)

ACCEPTED MANUSCRIPT

Fig. 3. Variations in Payenia whole rock major and trace elements. FeO/MnO vs. a) Zr/Sm, b) K/La, c) CaO and d) La/Nb. Data symbols as in Fig. 2. The Payenia data form trends indicating two-component mixing between high FeO/MnO Río Colorado high Nb/U-type pyroxenite melts and low FeO/MnO peridotite melts influenced by the subducting slab. The Río Colorado low Nb/U samples plot away from these trends towards higher Zr/Sm-K/La, constant La/Nb and lower CaO underlining that the low Nb/U component is not related to slab flux metasomatism. The inclusion data has not been shown here due to the large uncertainties on their FeO/MnO. Data sources as in Fig. 2 and from Bertotto et al. (2009), Dyhr et al. (2013a) and Holm et al. (2016).

Fig. 4. a) Backscattered electron microprobe image of olivine grain 2-4 (124570). Two generations of inclusions are seen. The darkest inclusion with the small sulfide globule (2-4 dark) is the most primitive inclusion and the others are later inclusions or embayments. The light halos around the inclusions are caused by the post-entrapment crystallization and the Fe-diffusion from the melt into the olivine before freezing. b) Inclusion 2-101 (124570) seen in transmitted light. Two gas bubbles and a sulfide globule is seen. c) Inclusion 4-151 (124567) seen in transmitted light. Several chromite crystals are seen on the walls of the inclusion

Fig. 5. a) Results of the Fe-diffusion modeling shown as modeled initial FeO in melt inclusions at time of trapping (FeOi) (filled symbols) vs. equilibrium olivine forsterite content. The unfilled symbols show the measured FeO-contents before correction. The black bars show the wr FeO-contents for each sample, and the bars outlined in black show the average FeOi for each sample calculated from the modeling results. Inclusion 2-58 has been omitted from the average because the grain is regarded as an antecryst. b) Modeling results for

ACCEPTED MANUSCRIPT

equilibration time in days vs. percent re-equilibration. c) Corrected CaO vs. MgO for inclusions. The filled symbols show the compositions corrected with the modeled FeOi-contents and calculated averages for the inclusions without modeling results. The unfilled symbols show the compositions corrected using the wr FeO^T-contents. The arrows indicate the two largest differences found in compositions calculated using wr FeO and modeled FeOi, respectively. d) The modeled profile for inclusion 4-109 (thin black line) shown together with the measured olivine profile as olivine forsterite content vs. distance from inclusion

Fig. 6. MgO vs. a) Al_2O_3, b) TiO_2, c) SiO_2, d) Na_2O, e) CaO, and f) K_2O (all in wt.%) for corrected inclusions (filled symbols), matrix compositions (no fill) and wr compositions of high and low Nb/U samples. Data for wrs are from Bertotto et al. (2009), Kay et al. (2013), Jacques et al. (2013) and Søager et al. (2013, 2015b). Reproducibility (2σ) on measurements of the VGA99 and VG568 (for K_2O) international standards are shown (Supplementary table B). The black lines are fractionation paths showing fractional crystallization of 8 % olivine to 6.5 wt.% MgO followed by 12.5 % fractionation of 80 % clinopyroxene + 20 % olivine to 5 % MgO. Wr high Nb/U sample 123972 (Søager et al., 2013) was used as starting composition and equilibrium olivine (assuming olivine $K_D^{(Fe/Mg)}$ = 0.30 and Fe^{2+}/FeO^T = 0.9) and clinopyroxene was subtracted in steps of 0.5 %.

Fig. 7. Primitive mantle normalized trace element diagrams of the measured inclusions, embayments and one matrix composition. a) sample 124567, b) sample CL467 and c) sample 124570. The wr compositions are shown for comparison as is high Nb/U inclusion 2-101 from sample 124570 in a). In b) and c), the grey fields show the compositions of the inclusions and embayments in sample 124567. Normalization values are from McDonough and Sun (1995)

ACCEPTED MANUSCRIPT

Fig. 8. K_2O vs. a) TiO_2, b) SiO_2, c) Cl, and d) P_2O_5, e) S (all in wt.%) and f) Dy/Yb_N (normalized to primitive mantle values from McDonough and Sun, 1995) of the corrected inclusions. The fields outline the wr compositions of the high Nb/U (full lines) and low Nb/U basalts (dashed lines) with Mg# > 55 (references as given in figure caption 5). Both inclusion and wr compositions were corrected for equilibrium olivine fractionation/accumulation to 10 wt.% MgO. The arrows outline the trends of the high and low Nb/U inclusions towards a high-K_2O component. In a), b) and d) the same fractionation model as in Fig. 5 showing 20.5 wt.% fractional crystallization of olivine and olivine +cpx for sample 123972 is shown in black.

Fig. 9. Nb/U vs. a) $(La/Sm)_N$ (normalized to primitive mantle values from McDonough and Sun, 1995), b) Th/U, c) Ti/Eu, d) Ce/Pb, e) La/Nb and f) Rb/Sr of the inclusions and measured embayments. However, embayments are not shown in f because their Rb/Sr has been changed by plagioclase fractionation. Fields for the wr compositions of the high and low Nb/U basalts are shown with references as in Fig. 5. The black lines show the fractionation paths formed by fractionation of 70 % clinopyroxene, apatite and rutile in the proportions 94:4:1, respectively, from the high Nb/U inclusion 5-28. The arrow in c) shows the effect of pure rutile fractionation. The partition coefficients for rutile and apatite are from Klemme et al. (2005) and Prowatke and Klemme (2006). The partition coefficients for Nb and Ta in rutile were arbitrarily set to 30 for both elements. Partition coefficients for clinopyroxene are from Green et al. (2000) (experiment 1802, 2 GPa), except for Pb which is from Lundström et al. (1998), K which is from Gaetani et al. (2003), and Th and U which are from Salters and Longhi (1999). The Rb partition coefficient in cpx was assumed equal to that of Ba. UCC is the global upper continental crust average from Rudnick and Gao (2003).

ACCEPTED MANUSCRIPT

Fig. 10. Multi element plots of low Nb/U wr sample 126230 (Søager et al., 2013) and inclusions 4-128 (sample 124567) and 5-33 (sample CL467). In a) divided by the concentrations of high Nb/U inclusion 5-28 (sample CL467) to show the enrichment relative to the high Nb/U component. The low Nb/U enrichment is largest in the elements Cs (not shown), Rb, Th, U and Pb, while the MREEs and HREEs are not enriched relative to the high Nb/U composition. The black line shows the modelled composition of inclusion 5-28 subtracted 50 % clinopyroxene by fractional crystallization. The yellow line shows 70 % fractionation of clinopyroxene, apatite and rutile in the proportions 94:4:1, respectively, from the high Nb/U inclusion 5-28. Partition coefficients as in Fig. 8. In b) normalized to primitive mantle values from McDonough and Sun (1995). For comparison is shown the composition of inclusion 5-28, a high-Nb basanite from Pilet et al. (2005) and a dataset of alkaline lamprophyres (Batki et al., 2014; Bayat and Torabi, 2011; Dostal and Owen, 1998; Harangi et al., 2003; Le Roex and Lanyon, 1998; Orejana et al., 2008; van der Meer et al., 2017). The low Nb/U samples have patterns similar to the alkaline lamprophyres.

Fig. 11. Na_2O/TiO_2 vs. a) K_2O, b) Al_2O_3/TiO_2, c) CaO/Al_2O_3, d) TiO_2, e) Na_2O, f) SiO_2 of the inclusions and wr high and low Nb/U samples compared to a dataset for alkaline lamprophyres and lamproiites. Only alkaline lamprophyres with Mg# > 60 and lamproiites with Mg# > 70 (calculated with $Fe^{2+}/FeO^T = 0.8$) are plotted and the inclusion and wr compositions are olivine fractionation corrected to 10 wt.% MgO. Mixing lines show mixing between wr sample 124564 (Søager et al., 2015b) and phlogopite lherzolite melt sta17 from Condamine and Médard (2014) (small bars), between wr sample 124564 and pyroxenite melt 40-E2 (Lambert et al., 2009) (asterisks) and between inclusion 5-28 and cpx-hornblendite melt AG7-4 (Pilet et al., 2008) (crosses). Tick marks are shown for every 10 % change in mixing proportions. The arrow in c) shows the effect of decreasing pressure on peridotite melt compositions. The fields show experimental melt compositions of peridotite

ACCEPTED MANUSCRIPT

(dashed outline) (1-3 GPa, F = 5-28 %, Hirose and Kushiro, 1993; Sorbadere et al., 2013; Walter, 1998), cpx-hornblendite melts (green outline) (Pilet et al., 2008), pyroxenite melts (red outline, only low degree melts are shown) (Lambert et al., 2009) and low-Si pyroxenite melts (black outline) (Hirschmann et al., 2003; Keshav et al., 2004; Kogiso and Hirschmann, 2006; Lambert et al., 2009). Phlogopite harzburgite (grey outlined fields) and phlogopite lherzolite melts are from Condamine and Médard (2014). In e) a field for the experimental melt compositions of Kogiso et al. (1998) formed at 1.5-2 GPa and 1300-1350°C is shown. These data largely fall within the peridotite fields in the other diagrams. Lamprophyre data references as in Fig. 9. Lamproiite data is from Prelević et al. (2005, 2008).

ACCEPTED MANUSCRIPT

ACCEPTED MANUSCRIPT

Highlights

- Melt inclusions from southern Payenia have highly variable element enrichment
- Magmas formed by mixing of asthenospheric high Nb/U and lithospheric low Nb/U melts
- Low Nb/U type inclusions are similar in composition to alkaline lamprophyres
- Low Nb/U melts were formed by fractionation of high Nb/U melts in the SCLM
- The percolative fractional crystallization involved cpx, rutile and apatite

ACCEPTED MANUSCRIPT

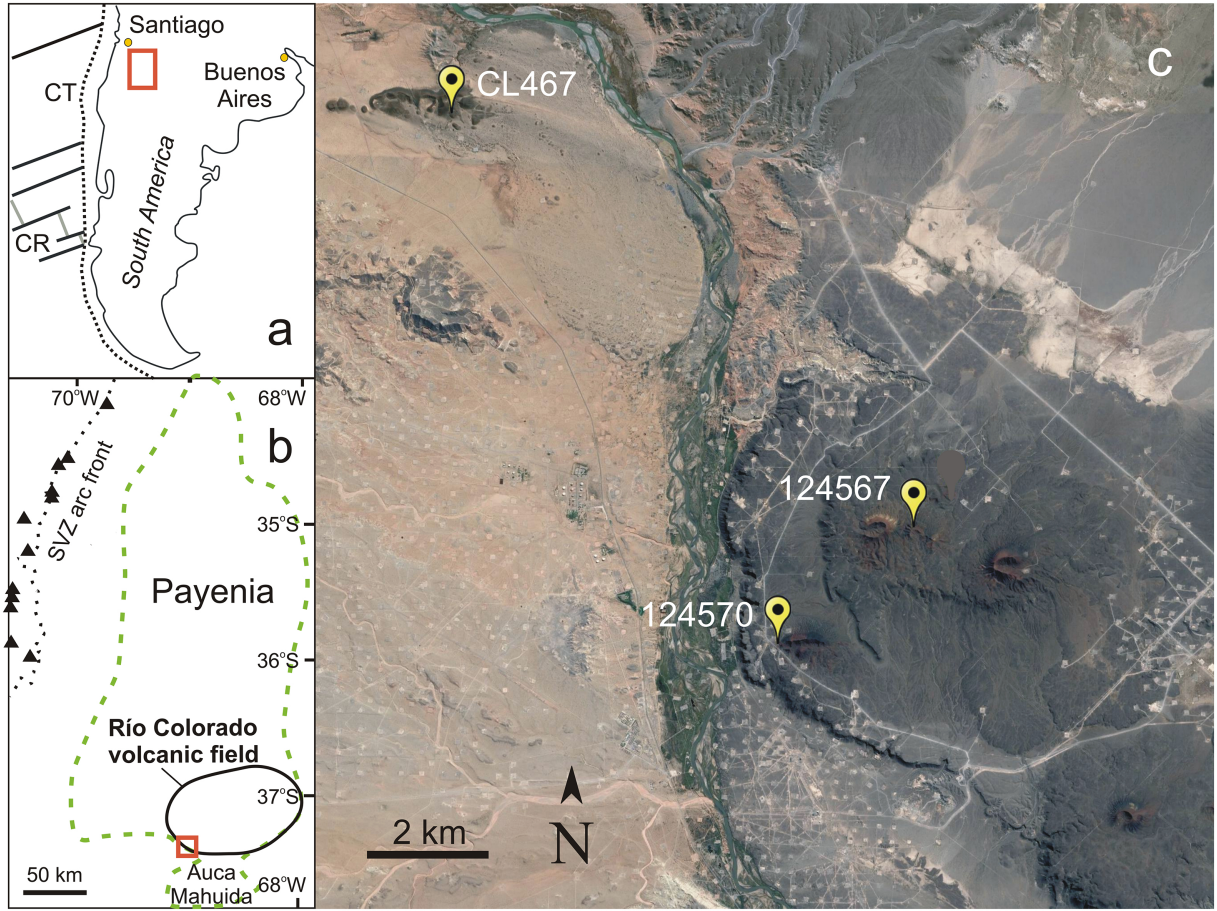
Santiago
CT
Buenos Aires
South America
CR
a
70°W
68°W
b
SVZ arc front
35°S
Payenia
36°S
Río Colorado volcanic field
37°S
50 km
Auca Mahuida
68°W
CL467
c
124567
124570
2 km
N

Figure 1

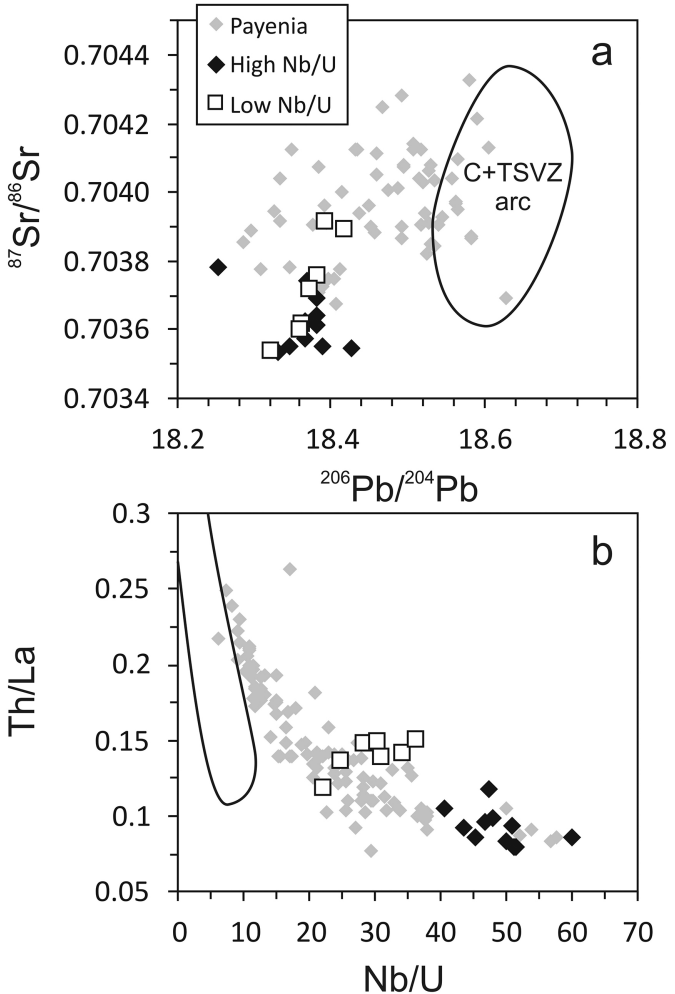
Payenia
High Nb/U
Low Nb/U
a
C+TSVZ
arc
0.7044
0.7042
0.7040
0.7038
0.7036
0.7034
87Sr/86Sr
18.2
18.4
18.6
18.8
206Pb/204Pb
b
0.3
0.25
0.2
0.15
0.1
0.05
Th/La
0
10
20
30
40
50
60
70
Nb/U

Figure 2

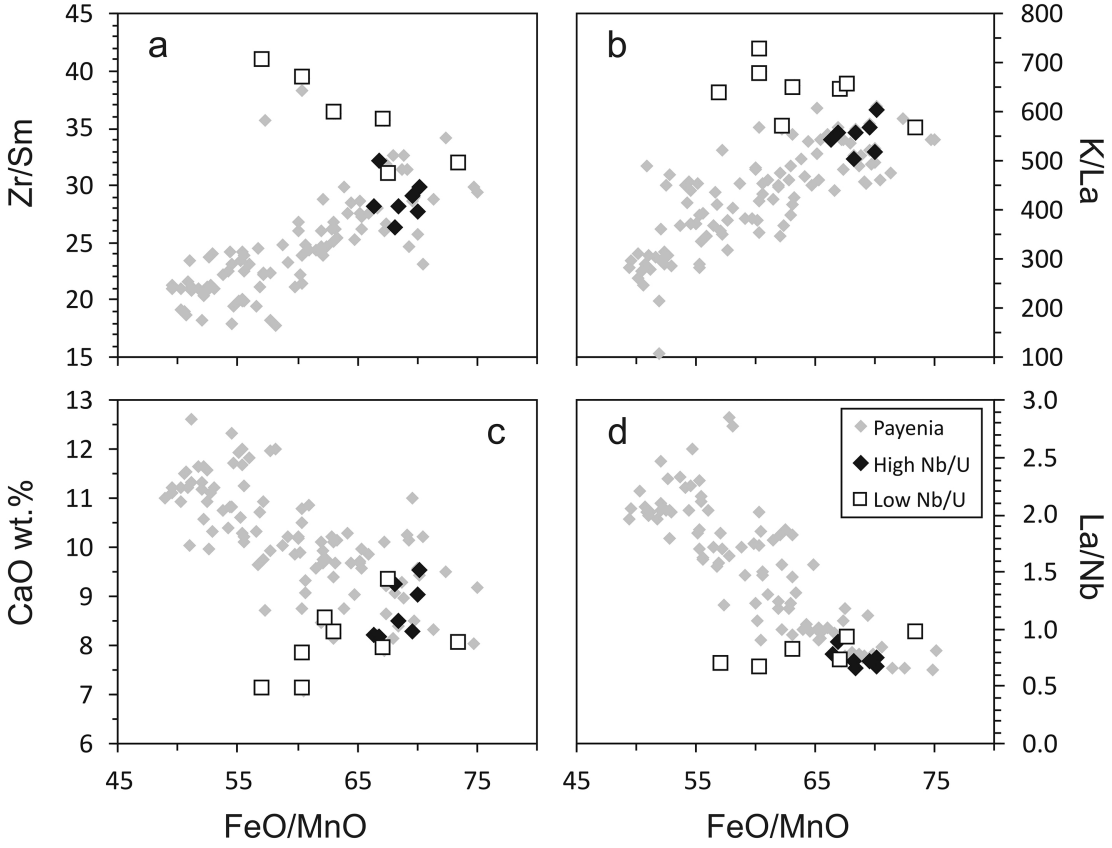
a
b
c
d
Zr/Sm
K/La
CaO wt.%
La/Nb
FeO/MnO
FeO/MnO
Payenia
High Nb/U
Low Nb/U
45
40
35
30
25
20
15
800
700
600
500
400
300
200
100
13
12
11
10
9
8
7
6
3.0
2.5
2.0
1.5
1.0
0.5
0.0
45
55
65
75

Figure 3

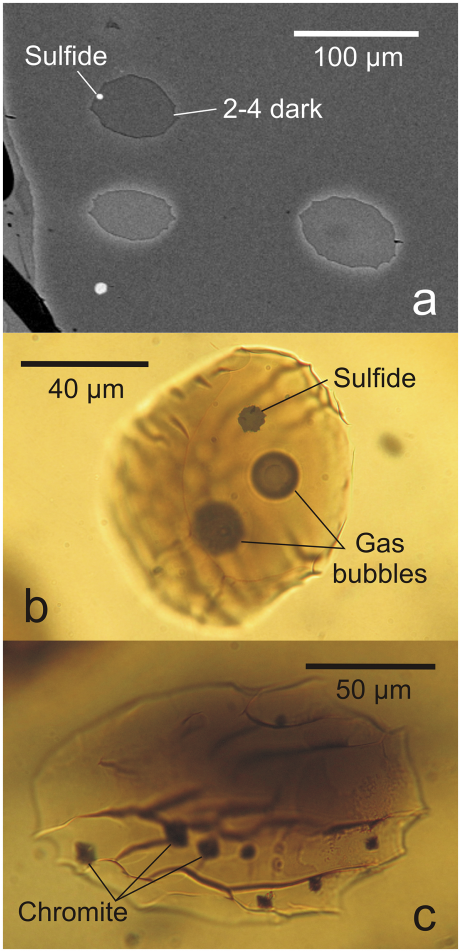
Sulfide
100 μm
2-4 dark
a
40 μm
Sulfide
Gas
bubbles
b
50 μm
Chromite
c

Figure 4

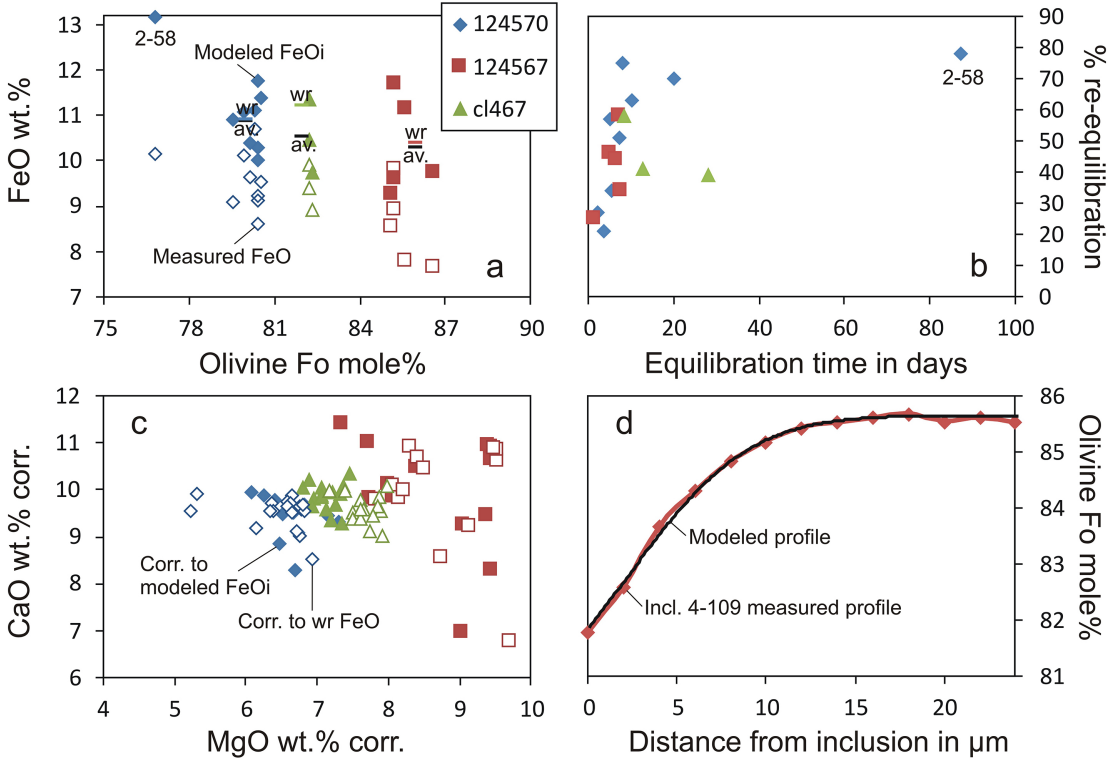
FeO wt.%
Olivine Fo mole%
2-58
Modeled FeOi
wr
av.
Measured FeO
124570
124567
cl467
a
% re-equilibration
Equilibration time in days
b
CaO wt.% corr.
MgO wt.% corr.
c
Corr. to modeled FeOi
Corr. to wr FeO
d
Modeled profile
Incl. 4-109 measured profile
Olivine Fo mole%
Distance from inclusion in µm

Figure 5

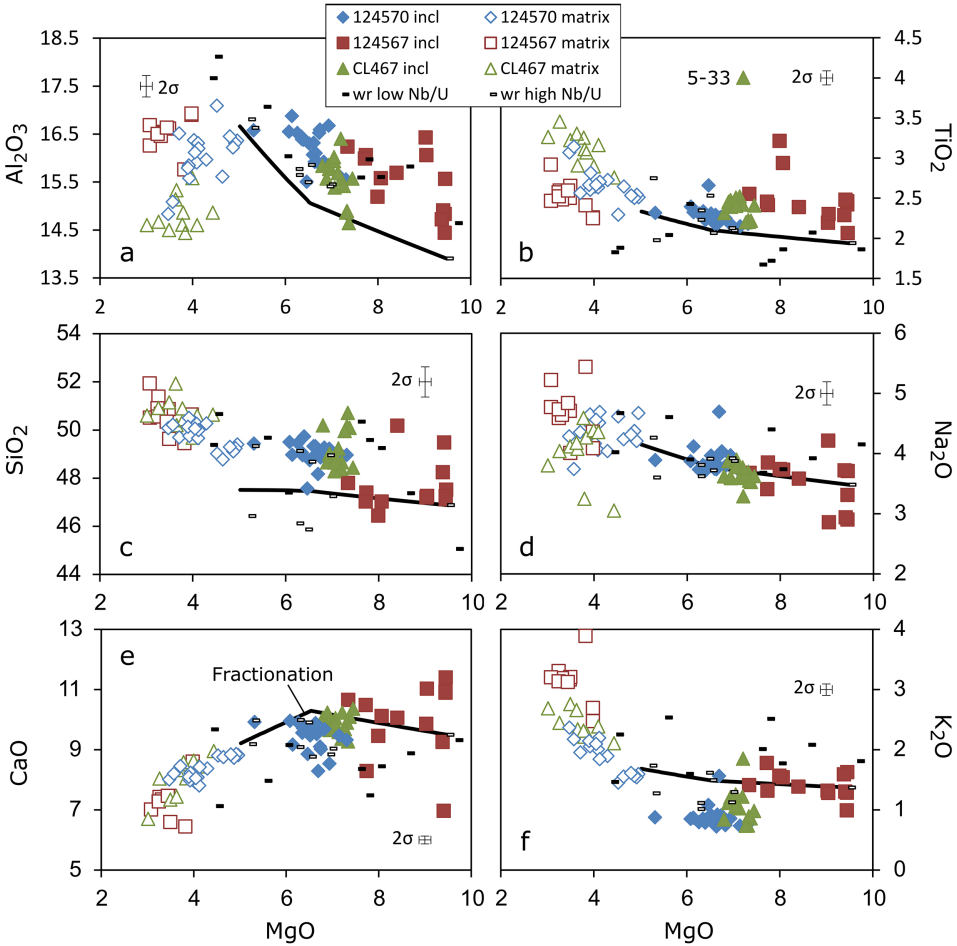
124570 incl
124570 matrix
124567 incl
124567 matrix
CL467 incl
CL467 matrix
wr low Nb/U
wr high Nb/U
Al2O3
TiO2
SiO2
Na2O
CaO
K2O
MgO
MgO
2σ
5-33
a
b
c
d
e
f
Fractionation

Figure 6

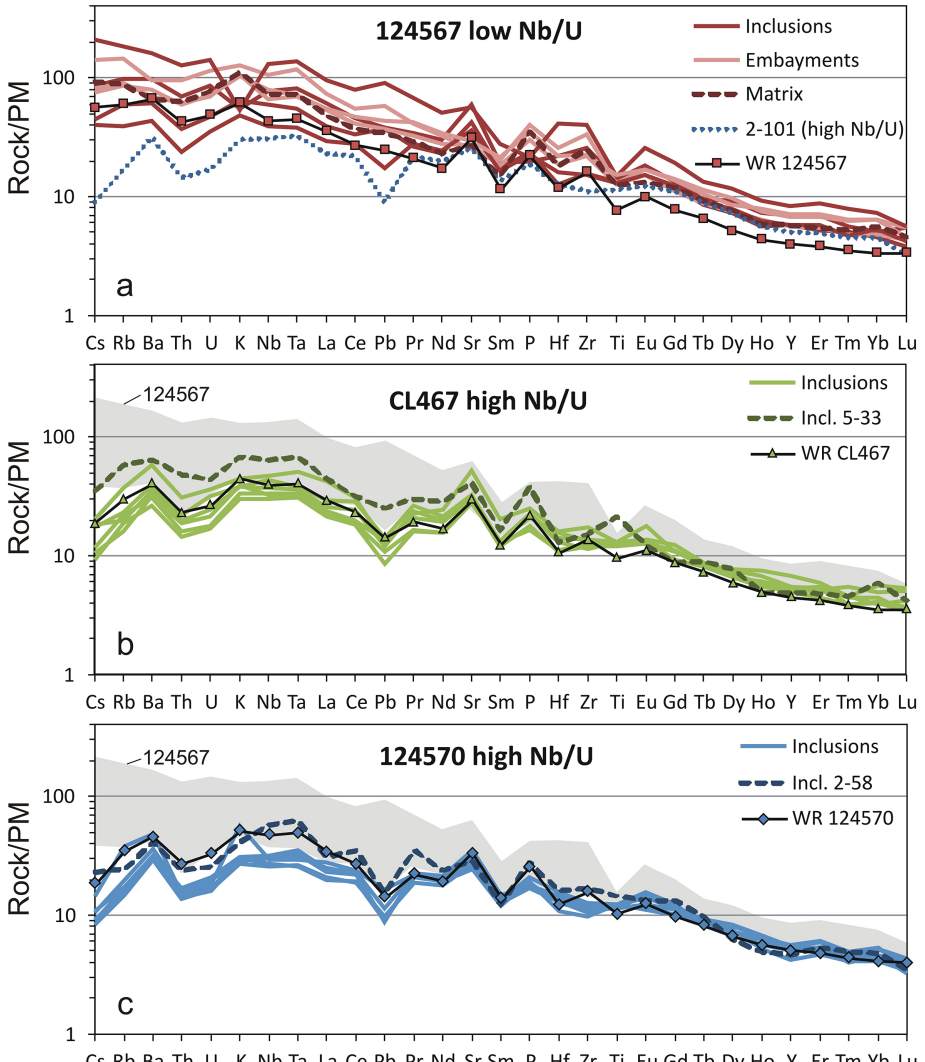
124567 low Nb/U
Inclusions
Embayments
Matrix
2-101 (high Nb/U)
WR 124567
Rock/PM
100
10
1
a
Cs Rb Ba Th U K Nb Ta La Ce Pb Pr Nd Sr Sm P Hf Zr Ti Eu Gd Tb Dy Ho Y Er Tm Yb Lu
124567
CL467 high Nb/U
Inclusions
Incl. 5-33
WR CL467
Rock/PM
100
10
1
b
Cs Rb Ba Th U K Nb Ta La Ce Pb Pr Nd Sr Sm P Hf Zr Ti Eu Gd Tb Dy Ho Y Er Tm Yb Lu
124567
124570 high Nb/U
Inclusions
Incl. 2-58
WR 124570
Rock/PM
100
10
1
c
Cs Rb Ba Th U K Nb Ta La Ce Pb Pr Nd Sr Sm P Hf Zr Ti Eu Gd Tb Dy Ho Y Er Tm Yb Lu

Figure 7

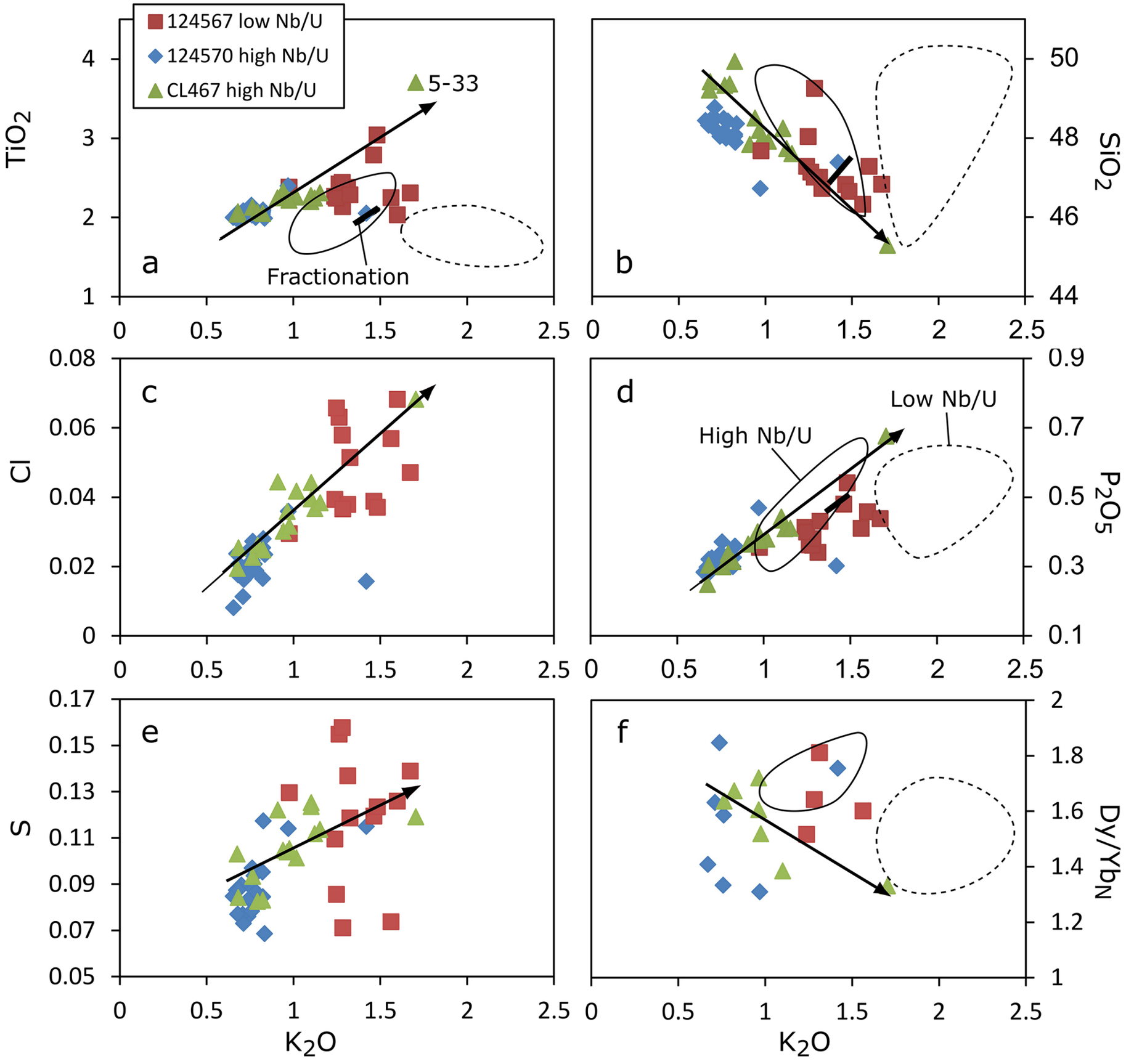
124567 low Nb/U
124570 high Nb/U
CL467 high Nb/U
5-33
Fractionation
a
b
c
d
e
f
High Nb/U
Low Nb/U
TiO2
SiO2
Cl
P2O5
S
Dy/YbN
K2O
K2O

Figure 8

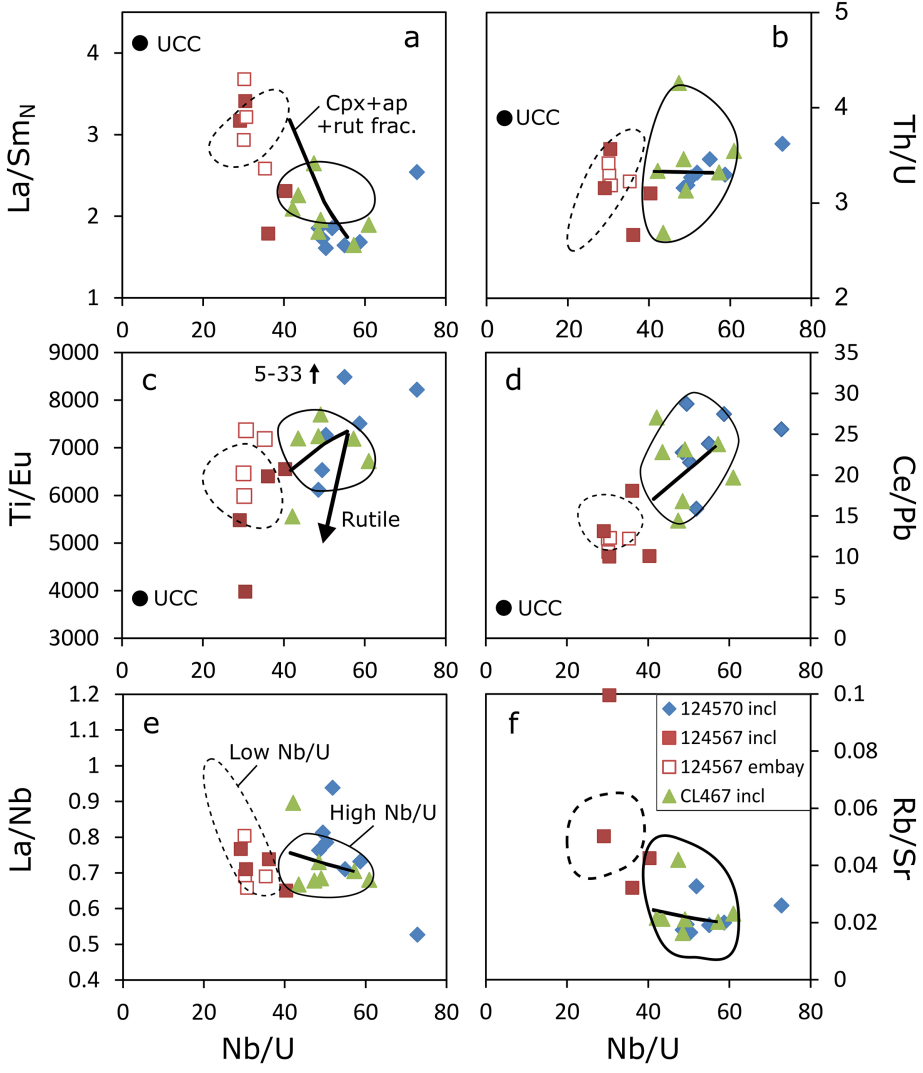
a
b
c
d
e
f
UCC
Cpx+ap
+rut frac.
5-33
Rutile
Low Nb/U
High Nb/U
124570 incl
124567 incl
124567 embay
CL467 incl
La/Sm$_N$
Th/U
Ti/Eu
Ce/Pb
La/Nb
Rb/Sr
Nb/U
Nb/U

Figure 9

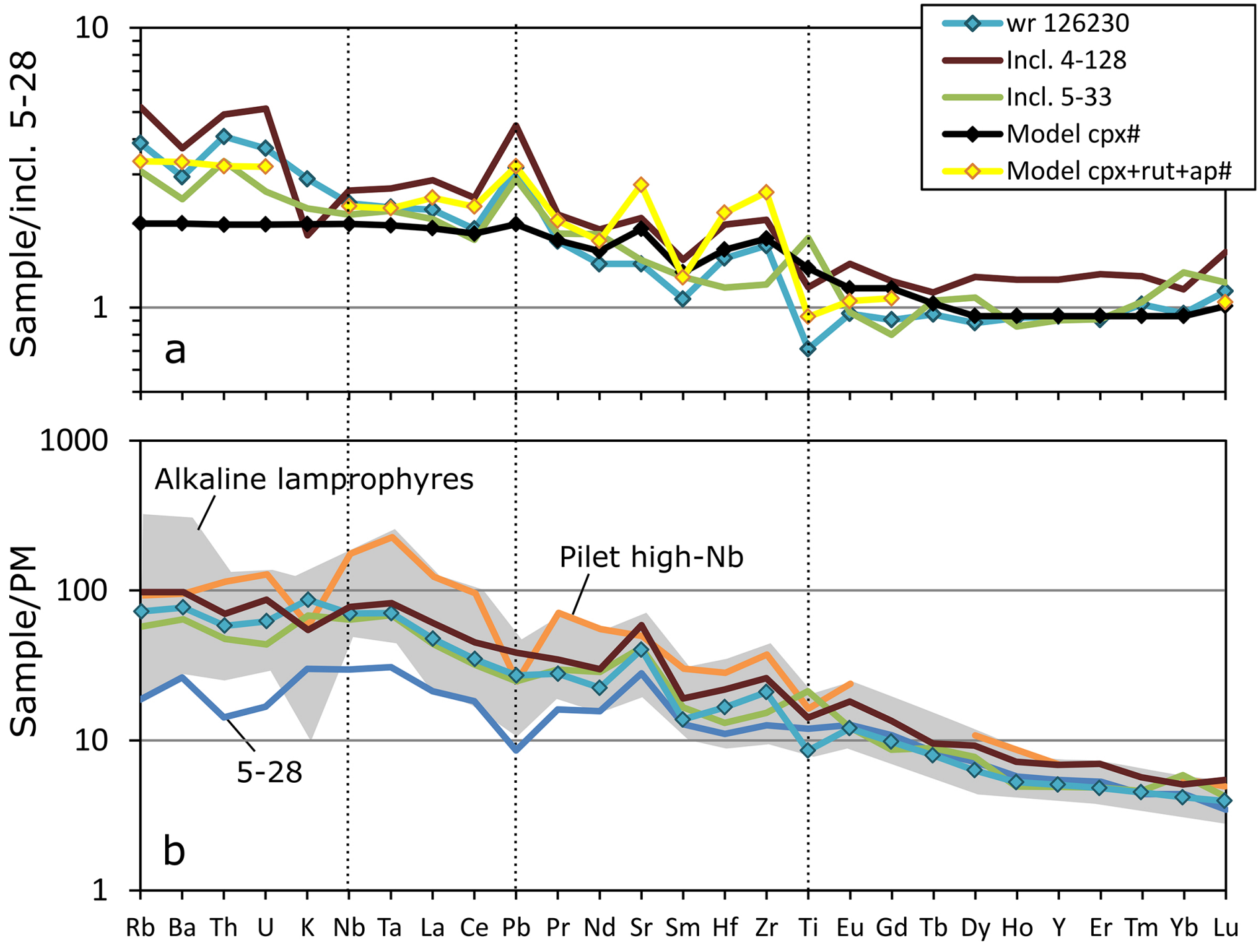
wr 126230
Incl. 4-128
Incl. 5-33
Model cpx#
Model cpx+rut+ap#
Sample/incl. 5-28
10
1
a
1000
100
10
1
Sample/PM
Alkaline lamprophyres
Pilet high-Nb
5-28
b
Rb Ba Th U K Nb Ta La Ce Pb Pr Nd Sr Sm Hf Zr Ti Eu Gd Tb Dy Ho Y Er Tm Yb Lu

Figure 10

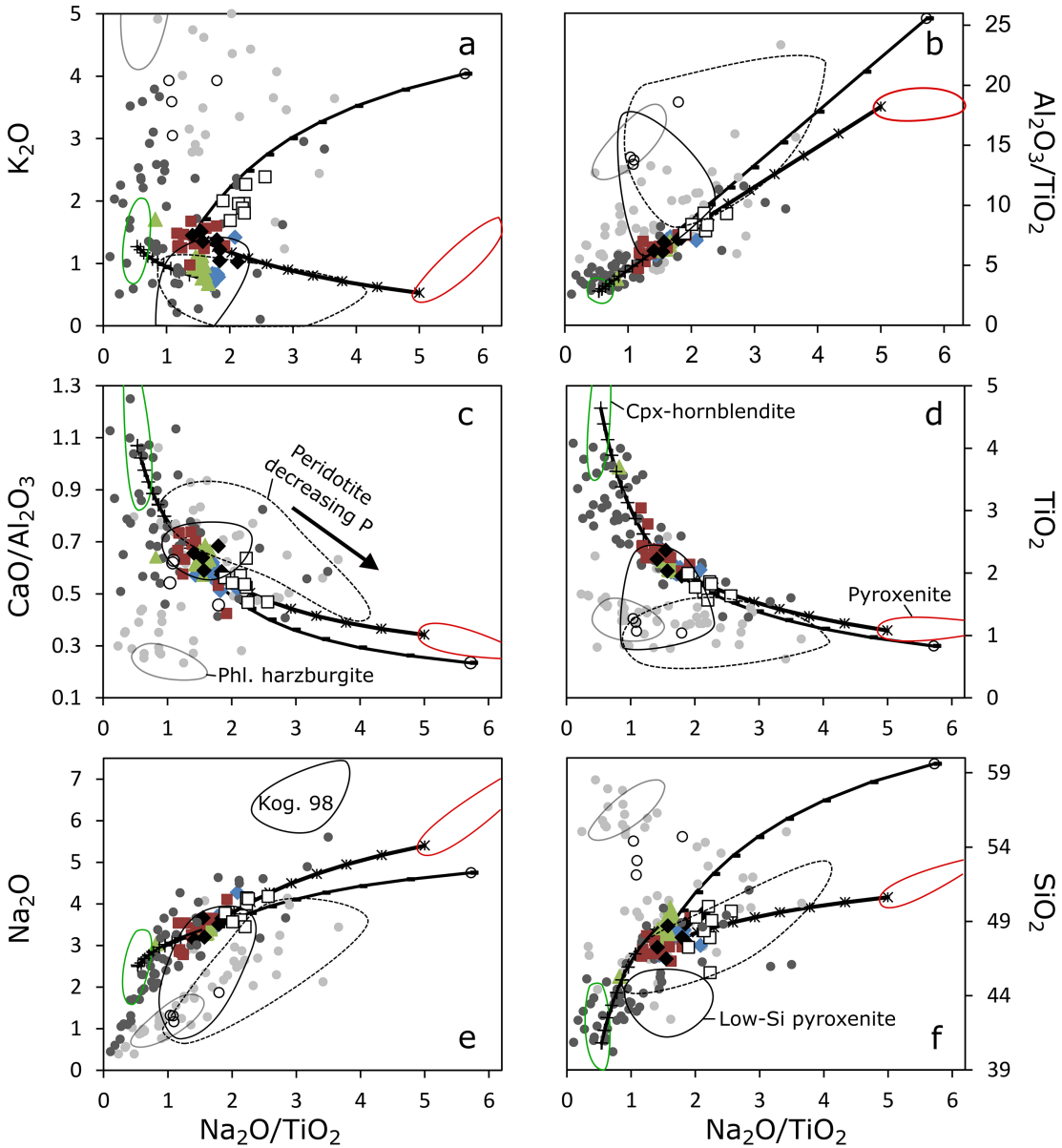
a
b
c
d
e
f
K_2O
Al_2O_3/TiO_2
CaO/Al_2O_3
TiO_2
Na_2O
SiO_2
Na_2O/TiO_2
Na_2O/TiO_2
Peridotite decreasing P
Phl. harzburgite
Cpx-hornblendite
Pyroxenite
Kog. 98
Low-Si pyroxenite
Alk. lamprophyres
Lamproiites
Phl. Lherz. melts
Incl. 124570
Incl. 124567
Incl. CL467
WR high Nb/U
WR low Nb/U
Mix phl. Lherz.
Mix pyroxenite
Mix cpx-hornbl.

Figure 11